Nilza Maria Lopes Ribeiro

Fibronectin and osteonectin adsorption onto hydroxyapatite nanostructures and its influence on osteoblast adhesion

Tese submetida à Faculdade de Engenharia da Universidade do Porto

para candidatura à obtenção do grau de Mestre em Engenharia Biomédica

Faculdade de Engenharia

Universidade do Porto

Julho 2009

This thesis was supervised by:

Professor Fernando Jorge Monteiro (supervisor)

Faculdade de Engenharia, Universidade do Porto

INEB – Instituto de Engenharia Biomédica, Laboratório de Biomateriais, Universidade do Porto

Doutora Susana R. Sousa (co-supervisor)

Instituto Superior de Engenharia do Porto, Politécnico do Porto

INEB – Instituto de Engenharia Biomédica, Laboratório de Biomateriais, Universidade do Porto

The research described in this thesis was conducted at:

INEB – Instituto de Engenharia Biomédica, Laboratório de Biomateriais

…to Susana Sousa

Acknowledgements

I would like to express my sincere gratitude to the persons who helped me during this project, and made this thesis possible.

I will start acknowledging my supervisors, Professor Fernando Jorge Monteiro and Doutora Susana Sousa for the opportunities they gave me, and for all of their help, support, patience, and friendship during the development of this work.

At INEB: I would like to express my sincere gratitude to all my remarkable colleagues and friends at INEB.

I am also very grateful to Lara Henriques, Manuela Brás and Ricardo Vidal for their support and for work collaboration in AFM, Zeta potential, Contact angle and Cell culture experiments.

Finally, I would like to express my sincere gratitude to Telmo, my parents and to my sister.

Abstract

Calcium phosphate biomaterials have been widely used in medical applications due to their exceptional properties of biocompatibility, bioactivity and osteoconductivity. Compared to conventional ceramic formulations, the properties of nanophased hydroxyapatite (nanoHA), such as surface grain size, pore size and wettability may control protein interactions and thus guide cellular responses. Considerable attempts have been made to modify the surfaces of materials using proteins, in order to enhance their cellular responses. The qualitative and quantitative assessment of the affinity of glycoproteins, like fibronectin, vitronectin, osteonectin or osteopontin, to nanophased HA model is essential to evaluate cell mechanisms involved in protein-surface interaction and thus to further improve the properties of implanted biomaterials. Human Fibronectin (FN) is a glycoprotein that plays an important role in cell attachment to biomaterials surfaces through its central-binding domain RGD sequence. Another glycoprotein that modulates cell proliferation and cellular interaction with ECM is osteonectin (ON), that unlike adhesive proteins such fibronectin, exhibits counter-adhesive effects during tissue repair and differentiation. Osteonectin, also termed as SPARC (secreted protein, acid and rich cystein) as a major non-collagenous bone ECM protein, is involved in multiple coordinated functions during bone formation (initiating mineralization and promoting mineral crystal formation). Bone osteonectin strongly binds to type I collagen and HA.

This work aimed at preparing and characterizing nanoHA surfaces sintered at two different temperatures, 725 ºC (HA725) and 1000 ºC (HA1000) for adsorption of two proteins, FN and ON. Another objective was to examine the influence of FN and ON pre-adsorption on MC3T3-E1 osteoblast cell adhesion cultured on HA725 and HA1000. It was found that the properties of the analyzed nanoHA substrates had an important role in the adsorption behavior of FN and ON. Particularly, the larger grain size, lower actual surface area and lower porosity present in HA1000 surfaces allowed a higher amount of both proteins to be adsorbed. Moreover the protein radiolabelling and immunofluorescence studies showed that FN molecules were weakly attached to HA725 surfaces, with a lower number of epitopes exposed. Regarding the cell culture results the osteoblast attachment / metabolic activity seems to be more sensitive to the nature of the surfaces than to the amount and type of adsorbed protein. Although, the effect of FN pre-adsorption improved the metabolic activity on HA1000 at 72 hrs and increased the number of adherent cells cultured on HA725 at 72 and 96 hrs. ON pre-adsorption seems not to influence osteoblast adhesion, for the concentrations used.

HA1000 substrates present similar behavior of cell viability and distribution of adherent osteoblast as the one found on TCPS cell culture material.

From the obtained results one can conclude that FN and ON adsorption patterns on nanoHA and subsequent response of osteoblast (cell metabolic activity and morphology), depends on the type of nanoHA substrate, being the HA1000 substrate a better candidate for bone tissue engineering than HA725.

Resumée

Les biomatériaux à base de phosphate de calcium sont très largement utilisés pour des applications biomédicales du fait de leurs propriétés exceptionnelles de biocompatibilité, bioactivité et d'ostéoconduction. En comparaison avec les céramiques conventionnelles, les propriétés de l'hydroxyapatite nanophasée (nanoHA), telles que la taille de grain, la taille de pore et la mouillabilité peuvent contrôler les interactions avec les protéines et orienter ainsi les réponses cellulaires. Par conséquent, en vue d'améliorer les réponses cellulaires, plusieurs tentatives ont été expérimentées pour modifier la surface de matériaux en utilisant des protéines. Le contrôle qualitatif et quantitatif de l'affinité des glycoprotéines comme la fibronectine, la vitronectine, l'ostéonectine ou l'ostéopontine, avec l'HA nanophasée modèle est essentiel pour évaluer les mécanismes cellulaires impliqués dans l'interaction protéine-surface et ainsi améliorer par la suite les propriétés des biomatériaux implantés.

La fibronectine humaine (FN) est une glycoprotéine qui joue un rôle important dans l'adhésion des cellules à la surface des biomatériaux par l'intermédiaire de sa séquence RGD. Une autre glycoprotéine modulant la prolifération cellulaire et l'interaction cellulaire avec la MEC est l'ostéonectine (ON), qui contrairement aux protéines d'adhésion telles que la fibronectine, a des effects anti-adhésifs au cours de la réparation tissulaire et de la différenciation. L'ostéonectine, également appelée SPARC (secreted protein, acid and rich cystein), qui est une des protéines essentielles de la MEC de l'os, est impliquée dans des fonctions multiples durant la formation de l'os (commençant la minéralisation et promouvant la formation du cristal minéral). L'ostéonectine de l'os se lie fortement au collagène de type I et à l'HA.

Ce travail a eu pour objectif la préparation et la caractérisation de surfaces nanoHA frittées à differentes températures, 725 °C (HA725) et 1000 °C (HA1000) pour l'adsoption de deux protéines, FN et ON. Un autre objectif a été d'examiner l'influence de la pré-adsorption de la FN et de l'ON sur l'adhésion cellulaire des ostéoblastes MC3T3-E1 cultivés sur HA725 et HA1000. Il a été démontré que les propriétés des substrats nanoHA analysés avaient un rôle important dans l'adsoption de la FN et de l'ON. En particulier, la plus grande taille de grain, la plus petite surperficie, et la plus petite porosité des surfaces HA1000 permet une plus grande quantité des deux protéines adsorbées. De plus, les études de radiomarquage et d'immunofluorescence ont montré que les molécules de FN étaient faiblement attachées aux surface HA725, avec un plus petit nombre d'épitopes exposés. En ce qui concerne les résultats de culture cellulaire, l'adhésion / activité métabolique des ostéoblastes semble plus

sensible à la nature des surfaces qu'à la quantité et au type de protéine adsorbée. Cependant, la pré-adsorption de la FN améliore l'activité métabolique pour HA1000 après 72 hrs et augmente le nombre de cellules adhérentes sur HA725 après 72 et 96 hrs. La pré-adsoption de ON ne semble pas influencer l'adhésion des ostéoblastes, pour les concentrations utilisés. Les substrats HA1000 ont montré des résultats de viabilité cellulaire et de morphologie des ostéoblates similaires à ceux obtenus avec du matériel de culture cellulaire TCPS.

D'après les résultats obtenus, il est possible de conclure que le mode d'adsoption de la FN et de l'ON sur les nanoHA et la réponse des ostéoblates qui en résulte (activité métabolique et morphologie), dépend du type de substrat nanoHA ; le substrat HA1000 étant un meilleur candidat pour l'ingénierie tissulaire de l'os que le HA725.

Resumo

Biomateriais de fosfato de cálcio têm sido utilizados em áreas de aplicação médica devido às suas propriedades excepcionais de biocompatibilidade, bioactividade, biodegradabilidade e osteocondutividade. Em comparação com a HA convencional, as propriedades físico-químicas da HA nanofásica (nanoHA) tais como o tamanho do grão de superfície, tamanho do poro, molhabilidade, podem controlar as interacções com as proteínas e assim aumentar a resposta celular. Neste aumento da resposta celular face à modificação das superfícies dos materiais implementados estão implicadas moléculas de adesão, daí que significativas tentativas têm sido feitas para modificar a superfície dos mesmos usando proteínas. O estudo qualitativo e quantitativo da afinidade de proteínas da matriz celular como a fibronectina, a vitronectina, a osteonectina ou a osteopontina num modelo de hidroxiapatite nanofásica pode ser essencial na avaliação dos mecanismos posteriores às interacções célula-superfície permitindo, deste modo, melhorar as propriedades de biomateriais implantados. A Fibronectin humana (FN) é uma glicoproteína que desempenha um papel importante na adesão das células às superfícies dos biomateriais através de uma sequência RGD do domínio central de ligação. Outra glicoproteína que medeia a proliferação e interacções das celulares com a ECM é a osteonectina (ON) que ao contrário das proteínas de adesão celular, como a fibronectina, têm um efeito de anti-adesão (counter-adhesive), durante os processos de renovação ou remodelação de tecidos. A osteonectina, também conhecida por SPARC (“secreted protein acidic and rich in cysteine”), como a proteína mais abundante das NCPs (proteínas não colagénicas) da matriz óssea está envolvida num conjunto de acções durante a formação do osso (mineralização inicial do osso e formação de cristais). A osteonectina do osso tem uma forte afinidade com o colagénio tipo I e a hidroxiapatite.

Este trabalho envolveu a preparação e caracterização de duas superfícies de nanoHA sinterizadas a duas temperaturas diferentes, 725 ºC (HA725) e 1000 ºC (HA1000) para adsorção de duas proteínas, FN e ON. Outro objectivo desta tese foi estudar a influência da pré-adsorção da FN e ON na adesão de osteoblastos MC3T3-E1 nas superfícies HA725 e HA1000. Os resultados demonstraram que as propriedades intrínsecas dos substratos de nanoHA estudados tiveram um papel importante na adsorção de FN e ON. Nomeadamente as superfícies HA1000 com grão de tamanho superior, área de superfície real menor e porosidade menor permitiram uma maior adsorção de ambas as proteínas. Através dos estudos de marcação

radioactiva e de imunofluorescência as moléculas de FN parecem estar fracamente aderentes às superfícies HA725 e com número inferior de epítopos expostos. De acordo com os resultados do estudo celular a adesão / actividade metabólica dos osteoblastos parecem ser mais sensível à natureza das superfícies do que ao tipo de proteína adsorvida. Contudo a pre-adsorção com FN aumentou a actividade metabólica nas superfícies HA1000 para 72 hrs, bem como o número de células aderentes nas superfícies HA725 para os tempos de cultura de 72 e 96 hrs. A pré--adsorção com ON parece não ter influência sobre a adesão celular, para as concentrações testadas. Os substratos HA1000 apresentaram um comportamento semelhante em termos de viabilidade e distribuição celulares ao encontrado nos TCPS.

A partir dos resultados obtidos pode se concluir que a adorção de FN e ON à nanoHA e subsequente resposta dos osteoblastos (adesão celular e morfologia), dependem do tipo de nanoHA substrato, sendo o substrato HA1000 o melhor candidato para engenharia de tecido ósseo do que o substrato HA725.

Contents

List of Figures

Chapter I

Chapter III

List of Tables

Chapter III

List of abbreviations

^{125}I	Iodine-125
^{125}I-FN	Radiolabelled fibronectin with iodine-125
^{125}I-ON	Radiolabelled osteonectin with iodine-125
AFM	Atomic force microscopy
BM-40	Basement membrane
BMPs	Bone morphogenetic proteins
BSA	Bovine serum albumin
CA	Contact angle
CCD	Charge-coupled device
DAPI	4', 6-diamino-2 phenylindole
ECM	Extracellular matrix
FBS	Fetal bovine serum
FGF	Fibroblast growth factor
FI	Fluorescence intensity
FN	Human plasma fibronectin
FT-IR	Fourier transform infrared technique
GDFs	Growth and differentiation factors
HA	Hydroxyapatite
IFM	Inverted epi-fluorescence microscope
ON	Osteonectin
PBS	Phosphate buffered saline
PDGF	Platelet-derived growth factor
RFU	Relative fluorescence units
RGD	Arg-Gly-Asp sequence
SA	Surface area
SD	Standard deviation
SEM	Scanning electron microscopy
Smax	Maximum peak with the depth of maximum valley
SPARC	Secreted protein, acidic and rich in cysteine
Sq	Root-mean-square
TCPS	Tissue culture polystyrene
TGF-β	Transforming growth factor
VEGF	Vascular endothelial growth factor
ZP	Zeta potential
α-MEM	Alpha minimum essential medium

Chapter I

Introduction

1 - Tissue Engineering. General Aspects

Tissue engineering is a recent field of interdisciplinary science and research that involves several scientific areas such as biochemistry, materials science and medicine. This area of research is interested in identifying the key parameters required for tissue regeneration to occur instead of tissue replacement. In bone tissue engineering one of the main interests is to obtain adequate scaffold materials, namely calcium phosphate based scaffolds that mimic the structure of biological apatite, bone bounding, and in some cases activate the genes expression in osteoblast-like cells to stimulate new bone growth. [1] These adaptable scaffolds may be adjusted in terms of composition and chemical stability, crystallinity, porosity and wettability or even be carriers of bioactive molecules, growth factors and/or living bone cells.

1.1 - Bone function and structure

Bone is a living conjunctive tissue composed by cells dispersed in bone matrix. This matrix is composed 40 % (wt %) of organic material and 60 % (wt %) of inorganic material, its ideal composition provides both flexibility and strength. All hard tissue of the human body is formed of calcium phosphates, except for small inner portions of the inner ear. The calcium orthophosphates occur mainly in the form of poorly crystallized non-stoichiometric Na-, Mg-, and carbonate-containing hydroxyapatite (biological apatite). Hydroxyapatite (HA, $Ca_5(PO_4)_3(OH)$, usually written as $Ca_{10}(PO_4)_6(OH)_2$) since the crystal unit cell comprises two molecules, has in its structure individual crystals with a plate-like morphology, 15-200 nm in length and 10-80 nm in width with a thickness between 2 and 7 nm. [2] The HA crystals of the mineral part are bound to collagen fibers (organic part). Bone tissue functions include support, protection and also provide the transformation of skeletal muscles contractions in useful movements. Bones can act as reserves of ions and above all play an important role in calcium metabolism. The

marrow, located within the medullar cavity of long bones and interstices of cancellous bone, produces blood cells and stem cells in a process called haematopoiesis.

1.2 - Bone cells

Bone tissue is composed by three cell types: osteoblasts, osteocytes and osteoclasts. (Fig. 1) Osteoblasts are located on the bone surfaces, side by side, and are responsible for the production of the organic part of bone matrix. Osteoblasts also manufacture hormones, such as prostaglandins, to act on the bone itself. They robustly produce alkaline phosphatase, an enzyme that has a role in the mineralization of bone, as well as many matrix proteins. Finally the osteoblasts become trapped and surrounded by bone matrix and originate the osteocytes. Osteocytes functions include formation of bone, matrix maintenance and calcium homeostasis.

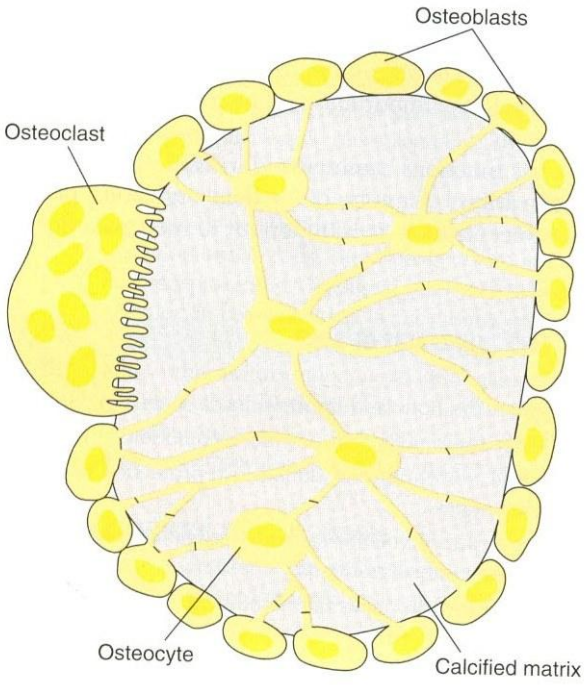

Fig. 1 – Cross section through a small portion of bone. The light gray area is mineralized osteoid. The osteocytes have long processes that extend through small canals and connect with each other and to osteoblasts via tight junctions. [3]

Osteoclasts are large multinucleated cells that are capable to secrete hydrogen ions, colagenases, and hydrolases, dissolving their own matrix and calcium phosphate. Therefore they are localized in areas where bone tissue resorption occurs (process included in the bone remodeling process that reduces its volume).

1.3 – Bone remodeling, healing and repair

The formation of bone includes a global action of biochemical cellular and hormonal processes, which permit a constant bone formation and resorption (bone remodeling). Bone morphogenetic proteins, (BMPs) and growth and differentiation factors, (GDFs) belong to a superfamily of proteins designed as transforming growth factor superfamily (TGF-β) that share a similar biological activity. These polypeptides mediate a number of physiological processes such as immune response, regulation of hormone secretion, growth and cell differentiation, morphogenesis, the regeneration of tissues and the induction and remodeling of bone.

1.4 – Nanostructured Hydroxyapatite

Calcium phosphate biomaterials have been widely used in dentistry and orthopedic applications in various physical forms: powders, granules, dense and porous blocks, injectable compositions, self-setting cements, coatings on metal implants, composites with polymers, etc. Despite their exceptional properties such as biocompatibility, bioactivity, biodegradability and osteoconductivity, they are not capable, as opposed to living tissues, to heal or restore the diseased tissues or organs by maintaining a blood supply, or modify their properties in response to environmental factors such as mechanical stress. Significant attempts have been made to produce synthetic biomaterials that closely mimic the HA crystals present in bone tissue. For the synthetic HA preparation several techniques has been employed, including hydrothermal reactions, sol-gel synthesis, pyrolysis of aerosols and micro-emulsion, biomimetic process, and chemical precipitation. The chemical precipitation is the most used alternative for the preparation of fine HA powders and was employed by Fluidinova S.A. to produce the nanoHA powders used in this work. [4] HA has been used as coating on orthopedic (e.g., hip joint prosthesis), and dental implants, as cement or added to some toothpastes as gentle polishing agent instead of calcium carbonate due to the chemical similarities to bone and teeth mineral enamel. Indeed the advances of the biomedical applications of calcium phosphates include the development of bioactive materials. Bioceramics made of dense HA revealed to be a good example of bioactive material which dissolve slightly and promote the formation of a layer of biological apatite before interfacing directly with the tissue at the atomic level, establishing direct chemical bond with bone. Such implants provide good stabilization for materials that are subject to mechanical stresses. However, when developing such

biomaterials for biomedical applications, it is very important to obtain a complete characterization to understand the biological interactions that occur at the bone tissue/material interface and to improve bone-forming biomaterials. Several studies have shown that structural characteristics, such as, specific surface area, pore volume or particle size of the synthetic biomaterials might influence their response in physiological environment, such as the biological apatite deposition and bone bounding. In particular, the properties of nanophased hydroxyapatite as compared to microphased ceramic (conventional ceramic), such as surface grain size, pore size and wettability may control protein interactions (like adsorption, conformation and bioactivity) and thus guide cellular responses (osteoblast adhesion and long term functionality expressed as proliferation, synthesis of alkaline phosphatase and deposition of calcium containing mineral).[5] Therefore the production of ceramics scaffolds for future applications in bone tissue engineering includes chemical and physical modifications such nanostructured and nanocrystalline materials made of HA, similar to the complex hierarchical structures of hard tissues (bone and teeth) and also modification of the materials surface using growth factors, living bone cells or proteins.[6]

2 - Extracellular Matrix

The extracellular matrix (ECM) is composed by four families of molecules: collagens, proteoglycans, glycoproteins and elastic proteins. While fibronectin acts as an adhesive protein, the most abundant protein in ECM, Type I collagen, has a structural function. Distinct matrixes can be found in different tissues. Bone has a solid ECM composed by collagen and crystals of calcium phosphate, a liquid ECM is found in blood and the connective tissue is constituted by soft ECM which may be loose or dense and rich in polysaccharides like in tendons. Collagen is the main compound present in the extracellular matrix providing in combination of proteoglycans the tissue mechanical integrity. The ECM can play many roles, such as providing support and anchorage for cells, segregating tissues from one another, and regulating intercellular communication. In concert with cell-intrinsic regulatory cascades, these temporally and spatially coordinated signals instruct cells to acquire specific fates, controlling for example cell division, differentiation, migration or apoptosis. Conversely, cells are constantly secreting signals that can trigger structural and biochemical microenvironment changes, as it is most evident during proteolytic remodeling of the ECM. The resulting reciprocal and dynamic cell-matrix interaction is crucial for tissue

development, maintenance and regeneration and may be involved in pathological situations such as tumor metastasis.

2.1 - Bone matrix Glycoproteins

Many bone matrix proteins as well as those in most ECM) are glycoproteins that contain oligosaccharide chains (glycans) covalently attached to their polypeptide side-chains presenting also motifs specifically recognized by cellular receptors. The glycoproteins designated traditionally by extracellular matrix proteins such as fibronectin, collagen, and vitronectin, are adhesive proteins and contribute to the structural stability of ECM. Another class of gycoproteins is the matricellular class of secreted glycoproteins including osteonectin, thrombospondins, tenascins or osteopontin can also support cell adhesion under some circumstances, but also exhibit counter-adhesive effects that lead to cell rounding and changes in cell shape that result in the disruption of cell-matrix interactions. Events that are characterized by changes in cell shape and mobility often require expression of these proteins, tissue renewal, and tissue remodeling and embryonic development. Osteoblast do not synthesize all the bone matrix proteins at the same time, instead the expression pattern of individual matrix proteins or their mRNAs vary spatially and temporally. [7] For example proteins like fibronectin and the osteonectin are expressed early in osteoblastic cell cultures undergoing mineralization in vitro, while osteocalcin is expressed only after the development of an established matrix. In this chapter brief description of fibronectin and osteonectin is presented since these proteins are an integral topic of this work.

2.2 - Fibronectin

The fibronectin protein is produced from a single gene, but alternative splicing of its pre-mRNA leads to the appearance of several isoforms. Fibronectin exists in two main forms: as an insoluble glycoprotein dimer that serves as a linker in the ECM (FN extracellular matrix), and as a soluble di-sulphide linked dimer found in the plasma (plasma FN). The plasma form is synthesized by hepatocytes, and the ECM form is produced by fibroblasts, chondrocytes, endothelial cells, macrophages, as well as by certain epithelial cells. Human Fibronectin (FN) is a large dimeric glycoprotein present in the ECM consisting of two almost identical polypeptide chains with a molecular weight around 250 kDa, linked by a pair of C-terminal di-sulphide bonds. Each sub-unit

has 60 nm in length and 2.5 nm in diameter, and is composed of three types of repeating modules (type I, type II and type III). All three modules are composed of two anti-parallel β-sheets; however, type I and type II are stabilized by intra-chain di-sulphide bonds, while type III modules do not contain any di-sulphide bridges. The absence of di-sulphide bonds in type III modules allows them to partially unfold under applied stress. The modules are arranged into several functional and protein-binding domains along the length of a fibronectin monomer. There are four fibronectin-binding domains, allowing fibronectin to be associated with other fibronectin molecules. The modules I_{4-5} along with the module I_{10-12} are involved in fibrin binding, an important event occurring during the formation of blood clots. The type I modules that surround the two type II modules assist in collagen binding. One of these fibronectin-binding domains, I_{1-5}, is referred to as the "assembly domain", and it is required for the initiation of fibronectin matrix assembly. [8] Like other FN modules, the type II module is found in a wide array of proteins, and is highly conserved. As previously referred, the two type II modules of fibronectin, along with surrounding type I modules, are exclusively involved in collagen binding. Modules III_{9-10} correspond to the "cell-binding domain" of fibronectin. The RGD sequence (Arg–Gly–Asp) is located in III_{10} and is the site of cell attachment via α5β1 and αVβ3 integrins on the cell surface (Fig. 2). [8] The "synergy site" is in III_9 and has a role in modulating fibronectin's association with α5β1 integrins. Fibronectin also contains domains for fibulin-1-binding (III_{13-14}), heparin-binding and syndecan-binding (III_{12-14}).

Fibronectin is known to play a role in several fundamental cell activities, as adhesion, growth, differentiation or migration. [9] In bone, fibronectin is involved in the early stages of osteogenesis and it has been suggested that it might be able to nucleate mineralization. [10, 11] Fibronectin has not only a prominent functional role in connective tissues but is also capable of interacting with a number of matrix components, including type I collagen, glycosaminoglycans, osteopontin and itself, does making it a central support of matrix architecture. Fibronectin is also involved in wound healing.

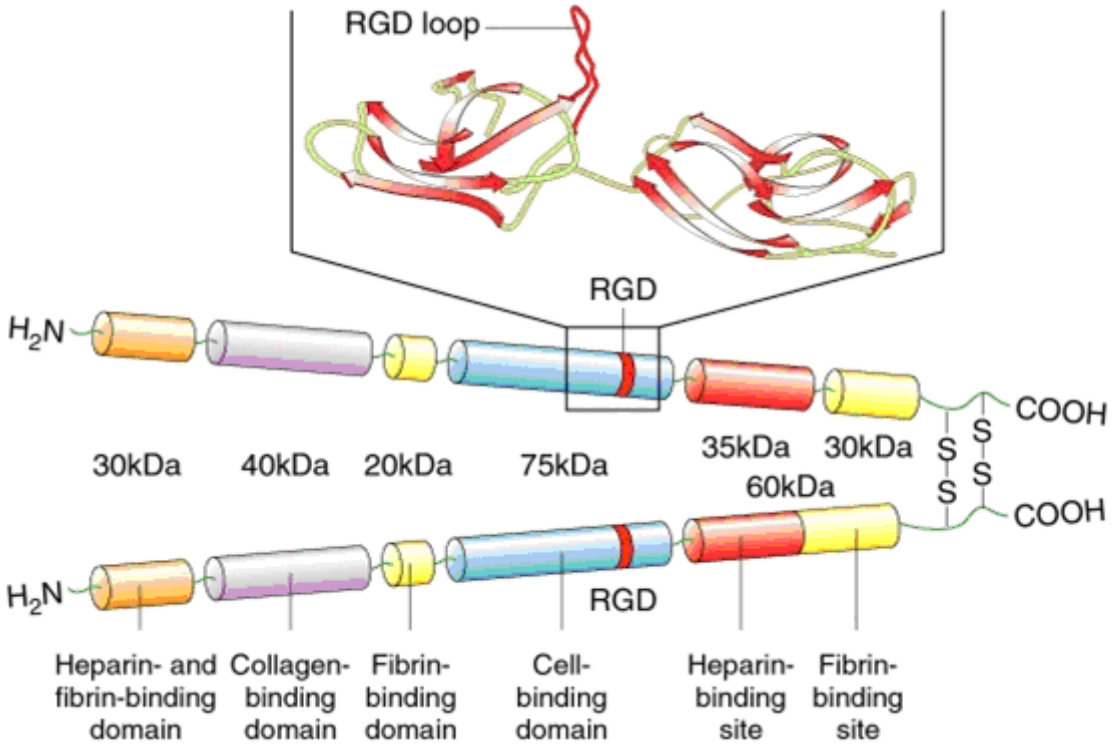

Fig. 2 - Schematic representation of fibronectin dimer showing its modular structure and functionality of various domains. Two subunits are shown, with amino termini to the left and carboxyl termini to the right. Regions implicated in adhesion and assembly are shown. [12]

Along with fibrin, plasma fibronectin is deposited at the injury site, forming a blood clot that stops bleeding and protects the underlying tissue. As repairing of the injured tissue continues, fibroblasts and macrophages begin to remodel the area, degrading the proteins that form the provisional blood clot matrix and replacing them with a matrix that more closely resembles the normal surrounding tissue. Fibroblasts secrete proteases, including matrix metalloproteinases, that digest the plasma fibronectin, and then the fibroblasts secrete cellular fibronectin and assemble it into an insoluble matrix. Fragmentation of fibronectin by proteases has been suggested to promote wound contraction, a critical step in wound healing. Fragmenting fibronectin further exposes its V-region, which contain the site for α4β1 integrin-binding. These fragments of fibronectin are believed to enhance α4β1 integrins-expressing cell binding, allowing them to adhere to and forcefully contract the surrounding matrix. Furthermore the fibronectin roles cover cell attachment and migration during the embryonic development. [13] In mammalian development, the absence of fibronectin leads to defects in mesodermal, neural tube, and vascular development.

The extensive structure-function analyses of FNs and their effects on cells in vitro may have relevance in optimizing a performance of biomaterials. The adsorption of fibronectin to different biomaterials substrates has been studied, exhibiting different conformations and directing different types of cellular responses on biomaterial surfaces. For example, some works have analyzed FN adsorption on hydroxyapatite surfaces and observed that the molecular structure of FN and its functional activity are depending on several factors as electrostatic energy between HA surface and the protein, surface chemistry, or the FN surface coverage. [14, 15]

2.3 - Osteonectin

SPARC (secreted protein, acidic and rich in cysteine), also termed osteonectin as a major non-collagenous protein of bone matrix, [16] or BM-40 as a component of the matrix of a basement membrane tumor is a member of the matricellular class of secreted glycoproteins that exhibit counter-adhesive effects that lead to cell rounding and changes in cell shape that result in the disruption of cell-matrix interactions. Events that are characterized by changes in cell shape and mobility often require expression of these proteins, such as tissue renewal, tissue remodeling and embryonic development. SPARC as a component of the matrix of a basement membrane tumor is a multifunctional calcium binding matricellular glycoprotein secreted by many different types of cells such as osteoblasts (during bone formation, initiating mineralization and promoting mineral crystal formation), fibroblasts, endothelial cells and platelets.[17] SPARC is a single-copy gene with a high degree of evolutionary conservation, has a molecular weight of 32.5 kDa and can be divided into three distinct modules as shown in Fig. 3. Module I (aa 3-51), previously termed domain I NH_2-terminal, is encoded by exons 3 and 4, contains immunodominant epitopes and binds to hydroxyapatite. The NH_2-terminal domain is an acidic region rich in asparagines (Asp) and glutamate (Glu) which can binds to 5-8 calcium ions, despite of the helix-turn-helix structural domain (EF-hand motifs), found in a large family of calcium-binding proteins, is present only in domain III. It is also the region that is the most distinct from other members of the SPARC gene family. Module II (aa 52-132), Cystein-rich, is encoded by exons 5 and 6 and contains two potential N-glycosylation sites, at asparagines 71 and 99. The sequence encodes a structure that is homologous to a repeated domain in follistatin, a protein that has affinity to members of the TGF-β superfamily. Module II also contains bioactive peptides that exert different effects on endothelial cells. Peptide 2.1 (aa 55-74), part of the EGF-like β hairpin, inhibited the proliferation of endothelial cells.

Peptide 2.3 (aa 113-130), is homologous to Kazal serine protease inhibitors family, stimulating endothelial cell proliferation and angiogenesis. [18] Additionally, it has been suggested that the NH_2-terminal region of module II binds to heparin or to proteoglycans. [19]Module III (aa 133-285), formerly designated as domains III and IV, is encoded by exons 7 and 9. Its structure is globular and contains two EF-hand motifs which bind to extracellular Ca^{2+}. This module also contains a sequence designated as peptide 4.2 (aa 254-273), which has been shown to bind to endothelial cells and to inhibit their proliferation. [20] The fibril-forming collagen types I, III, and V, and the basement membrane collagen type IV, bind to the module III of SPARC in a Ca^{2+} dependent fashion. Analysis of the crystal structure and site-directed mutagenesis within module III demonstrated that five residues R149, N156, L242, M245, and E246.are required for collagen binding. The functional significance of the interaction of SPARC with collagens in tissues is not clear. Collagen may serve as a storage site for SPARC in the ECM or might directly modulate the activity of SPARC, its counter-adhesive or anti-proliferative function.

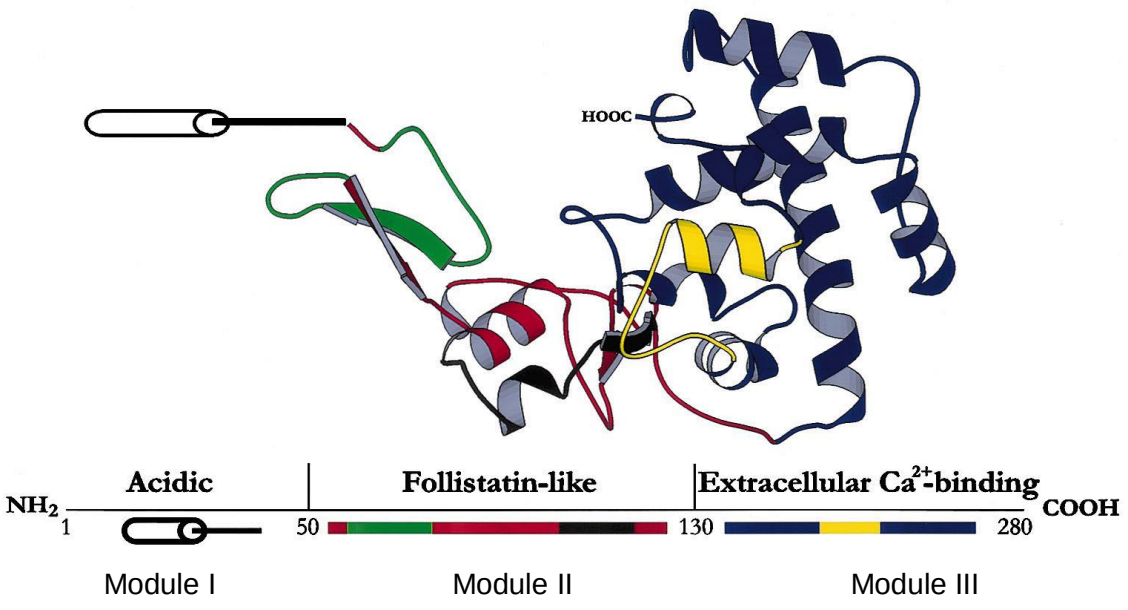

Fig. 3 - Structure of human SPARC protein. A ribbon diagram derived from crystallographic data shows the three modular domains of SPARC The follistatin-like domain, aa 53-137, shown in red, except the peptide 2.1, aa 55-74 and the (K)GHK angiogenic peptide (amino acids 114–130) shown in green and black, respectively. Module III,I aa 138-286 is shown in blue, except the amino acids 255–274 (peptide 4.2) shown in yellow. Modified from Ref. [19]

The expression pattern of this protein has provided clues to its potential capabilities. *In vitro* experiments provided evidence that SPARC [21]:

a) has a counter-adhesion effect on cells, since it disrupts the cell adhesion to extracellular matrix by its bond to EMC proteins structural, as collagen and vitronectin;

b) promotes morphologic changes in cell shape;

c) inhibits the cell cycle, namely, makes cells to reside in G1 phase of cellular cycle;

d) regulates cell differentiation;

e) inactivates cellular responses to certain growth factors, regulates the activity of growth factors, such platelet-derived growth factor (PDGF), Fibroblast growth factor (FGF) or the Vascular endothelial growth factor (VEGF); [20]

f) regulates ECM and matrix metalloprotease production.

In addition to the described functions, SPARC-null mice are born with no obvious abnormalities, shortly after birth the mice undergo progressive early-onset cataractogenesis; thus, the SPARC gene is necessary for lens transparency. Osteonectin has a strong affinity for HA even in the presence of guanidine and urea. This protein binds to the ECM proteins like types I, III, IV and V collagen, thrombospondin, PDGF-AB e o PDGF-BB. It has been shown that bone osteonectin strongly binds to type I collagen and synthetic HA and can mediate the in vitro mineralization of the type I collagen. [16] Therefore this protein is involved in bone initiating mineralization process; it is responsible for the initiation of the crystallization of Ca^{2+} and phosphate. It appears that osteonectin has a role in connected collagen fibers to HA crystals by a terminal sequence rich in amino acids. On the other hand, post-translational modification of osteonectin may be controlled in a tissue specific manner and further potentially associated with functions of osteonectin. Interestingly, the bone and platelet osteonectins have patterns of glycosylation that appeared to affect collagen binding activity. Specifically, bone osteonectin binds to types I, III and V collagen and platelet osteonectin has no apparent affinity for them. [22] Several applications for osteonectin have been tried in the development of advanced nanocomposites for skeletal tissue regeneration. One example of this kind of application (Fig. 4) was the use of a glutamic acid-rich peptide (a sequence of six glutamic acids) derived from osteonectin, functionalized with an acrylate group for covalent attachment to the matrix that significantly increased the shear modulus of a bone-mimetic hydrogel/apatite nanocomposite and improved the dispersion of apatite nanoparticles in aqueous solution. [23]

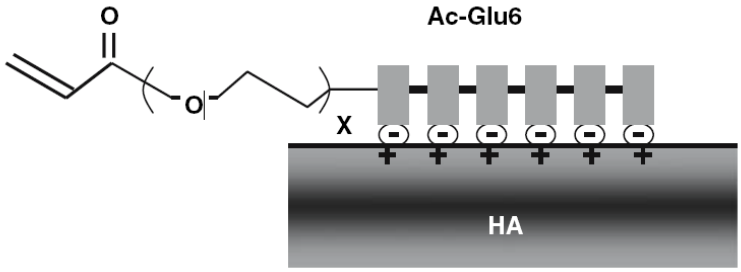

Fig. 4 - Schematic diagram illustrating the ionic interaction between Ac-Glu6 peptide and HA nanoparticle. Terminal acrylate group of the Ac-Glu6 provides an unsaturated group for covalent crosslinking of the peptide to the PLEOF matrix, while Glu6 provides a sequence for physical attachment to HA nanoparticles. [23]

The qualitative and quantitative assessment of the affinity of glycoproteins, like fibronectin or osteonectin, to nanophase HA model is essential to evaluate cell mechanisms involved in protein-surface interaction and thus to further improve the properties of implanted biomaterials. The aim of this work was to study the adsorption of two proteins, FN and ON, and their influence on MC3T3-E1 osteoblast cell adhesion to two types of nanoHA discs. The substrates were characterized in terms of surface morphology, zeta potential, roughness, wettability, porosity, and relative amount of adsorbed protein. FN conformation and ON affinity were also evaluated. Finally cell adhesion, distribution and morphology on the two nanoHA substrates were also followed.

REFERENCES

1. Griffith LG, Naughton G. Tissue engineering - Current challenges and expanding opportunities. Science 2002 Feb;295(5557):1009.

2. Fratzl P, Gupta HS, Paschalis EP, Roschger P. Structure and mechanical quality of the collagen-mineral nano-composite in bone. J Mater Chem 2004;14(14):2115-2123.

3. Vander AJ. Human physiology:the mechanisms of body function. In: Vander AJ, Sherman J, Luciano D, editors. 7th ed, 1993. p. 536.

4. Mateus AYP, Barrias CC, Ribeiro C, Ferraz MP, Monteiro FJ. Comparative study of nanohydroxyapatite microspheres for medical applications. J Biomed Mater Res Part A 2008 Aug;86A(2):483-493.

5. Manuel CM, Foster M, Monteiro FJ, Ferraz MP, Doremus RH, Bizios R. Preparation and characterization of calcium phosphate nanoparticles. In: Barbosa MA, Monteiro FJ, Correia R, Leon B, editors. 16th International Symposium on Ceramics in Medicine; 2003 Nov 06-09; Porto, PORTUGAL: Trans Tech Publications Ltd; 2003. p. 903-906.

6. Jun IK, Jang JH, Kim HW, Kim HE. Recombinant osteopontin fragment coating on hydroxyapatite for enhanced osteoblast-like cell responses. J Mater Sci 2005 Jun;40(11):2891-2895.

7. Majeska RJ. Cell Biology of Bone. In: Cowin SC, editor. Bone Mechanics Handbook. 2nd ed, 1934. p. 2-3.

8. Wierzbicka-Patynowski I, Schwarzbauer JE. The ins and outs of fibronectin matrix assembly. J Cell Sci 2003 Aug;116(16):3269-3276.

9. Geiger B, Bershadsky A, Pankov R, Yamada KM. Transmembrane extracellular matrix-cytoskeleton crosstalk. Nat Rev Mol Cell Biol 2001 Nov;2(11):793-805.

10. Globus RK, Doty SB, Lull JC, Holmuhamedov E, Humphries MJ, Damsky CH. Fibronectin is a survival factor for differentiated osteoblasts. J Cell Sci 1998 May;111:1385-1393.

11. Moursi AM, Damsky CH, Lull J, Zimmerman D, Doty SB, Aota SI, et al. Fibronectin regulates calvarial osteoblast differentiation. J Cell Sci 1996 Jun;109:1369-1380.

12. Cella. Cell biology. Shaoxing college of life sciences college of arts and sciences, 2006.

13. Pankov R, Yamada KM. Fibronectin at a glance. J Cell Sci 2002 Oct;115(20):3861-3863.

14. Shen J-W, Wu T, Wang Q, Pan H-H. Molecular simulation of protein adsorption and desorption on hydroxyapatite surfaces. Biomaterials 2008;29(5):513-532.

15. Pellenc D, Gallet O, Berry H. Adsorption-induced conformational changes in protein diffusion-aggregation surface assemblies. Phys Rev E 2005 Nov;72(5):9.

16. Termine JD, Kleinman HK, Whitson SW, Conn KM, McGarvey ML, Martin GR. Osteonectin, a bone-specific protein linking mineral to collagen. Cell 1981;26(1):99-105.

17. Brekken RA, Sage EH. SPARC, a matricellular protein: at the crossroads of cell-matrix. Matrix Biol 2000 Dec;19(7):569-580.

18. Lane TF, Sage EH. The biology of SPARC, a protein that modulates cell-matrix interactions. Faseb J 1994 Feb;8(2):163-173.

19. Hohenester E, Maurer P, Timpl R. Crystal structure of a pair of follistatin-like and EF-hand calcium-binding domains in BM-40. Embo J 1997 Jul;16(13):3778-3786.

20. Kupprion C, Motamed K, Sage EH. SPARC (BM-40, osteonectin) inhibits the mitogenic effect of vascular endothelial growth factor on microvascular endothelial cells. J Biol Chem 1998 Nov;273(45):29635-29640.

21. Yan Q, Sage EH. SPARC, a matricellular glycoprotein with important biological functions. 50th Annual Meeting of the Histochemical-Society; 1999 Apr 16-17; Bethesda, Maryland: Histochemical Soc Inc; 1999. p. 1495-1505.

22. Kelm RJ, Mann KG. The collagen binding-specificty of bone and platelet osteonectin is related to differences in glycosylation. J Biol Chem 1991 May;266(15):9632-9639.

23. Sarvestani AS, He X, Jabbari E. Osteonectin-derived peptide increases the modulus of a bone-mimetic nanocomposite. Eur Biophys J Biophys Lett 2008 Feb;37(2):229-234.

Materials and Methods

1 - Preparation and characterization of nanohydroxyapatite discs

Nanohydroxyapatite (nanoHA) was kindly supplied by Fluidinova S.A. (Portugal), (nanoXIM•HAp202). Cylindrical hydroxyaptite (HA) discs were obtained using 75 mg of dry powder under uniaxial compression stress of 40 bar (Mestra snow P3). Two different sintering temperatures were used, namely 725 ºC (HA725) and 1000 ºC (HA1000) during 15 min with a heating rate of 20 ºC/min. The sintering cycle was completed with a cooling process inside the furnace. The mass of the nanoHA discs was assessed by using an analytical balance (Metler AG285). The diameter and thickness of the discs were measured with a digital caliper (Duratool). All the experimental conditions previously referred were optimized in order to have stable discs conserving a nanoscale grain dimension.

Chemical characterization of nanoHA was performed by Fourrier transformed infrared (FT-IR) spectroscopy, using a Perkin-Elmer 2000 FT-IR spectrometer. For that purpose HA725 and HA1000 discs were reduced to powder and analyzed as KBr pellets at a spectral resolution of 2 cm^{-1}. The original nanoHA powder was also analyzed by a similar methodology. One hundred scans were accumulated per sample.

The zeta potential (ZP) of HA725 and HA1000 powders was measured using a ZetaSizer Nano ZS, applying the auto mode method. This unit automatically calculates the electrophoretic mobility (UE), and the ZP of the particle analyzed according to Henry's equation:

$$UE = 2\varepsilon z f(ka)/3\eta \qquad (1)$$

where z is the ZP, UE the electrophoretic mobility and f(ka) the Henry's function. Measurements were performed at pH 7.4, in deionized water and three different 0.01M electrolyte solutions, KNO_3, NaCl and KCl, using a sample concentration of 0.1 g/L.

2 - Surface characterization of nanohydroxyapatite discs

The surface characterization of HA discs was performed using contact angle measurements (CA), scanning electron microscopy (SEM), and atomic force microscopy (AFM). The surface area and pore characterization were evaluated by Mercury intrusion porosimetry.

Wettability studies were performed using a contact angle measuring system from Data physics Instruments GmbH, Germany, model OCA 15, equipped with a video charge-coupled device (CCD) camera, an electronic syringe unit (Hamilton) and SCA 20 software. Ultrapure water was used with resistivity not higher than 18.2 MΩ.cm. Contact angles were obtained by the sessile drop method, at 25 ºC in a chamber saturated with the liquid sample. Digital images were recorded every 40 ms up to 30 s by the CCD-camera. Because of the absorbing nature of the nanoHA discs the contact angle was calculated at the moment when the drop (2 µL of ultrapure water) contacted the surface by applying the tangent function. Results reported are the average ± standard deviation (SD) of at least 15 measurements (one per sample).

SEM analyses were performed using a FEI Quanta 400FEG/EDAX Genesis X4M microscope under high vacuum conditions. HA, HA1000 and HA725 discs were sputter-coated with a thin gold film, using a sputter coater (SPI-Module) in an argon atmosphere before analysis.

The Atomic Force Microscopy (AFM) measurements were taken using a PicoPlus scanning probe microscope interfaced with a Picoscan 2500 controller (both from Molecular Imaging). Each sample was imaged with a 10x10 μm^2 piezoscanner. Imaging and roughness analysis were performed at room temperature, in Tapping mode®, using a silicon cantilever with a spring constant of 25-75 N/m. Three samples of each type were analyzed at three randomly chosen locations. The surface roughness was obtained from scanned areas of 2500x2500 nm^2 using the SPIP software. To characterize the roughness, root-mean-square roughness (Sq) was obtained as well as the maximum peak with the depth of the maximum valley (Smax). The diameters of twenty grains randomly chosen were measure from the AFM images of HA725 and HA1000 discs. The results referred to surface roughness and the diameter measurements; correspond to the mean ± SD.

Mercury porosimetry (Quantachrome Poremaster model No. 60) was used to assess the porosity and the actual surface area for both types of sintered discs (HA725 and HA1000). In this procedure, 0.4 g of each dried material was penetrated by mercury at high pressure and the data reported were obtained using Quantachrome Poremaster for Windows, versions 3.0 and 4.02.

3 - Protein solutions

Human plasma fibronectin (FN), (Sigma, ref. F-0895) and Secreted Protein Acidic and Rich in Cysteine (SPARC), also termed osteonectin, from mouse parietal yolk sac (Sigma, ref. S5174) solutions were prepared by dilution in phosphate buffered saline, (PBS; Sigma, pH = 7.4, ref. P-3813) at concentrations of 20.0 µg/mL and 10 µg/mL, respectively, for the AFM, Radiolabelling, Immunofluorescence and Cell culture studies. The exchangeability of the adsorbed FN was also evaluated using FN (20.0 µg/mL), SPARC (0.02 µg/mL) and 10 % plasma solutions. The latter protein concentrations correspond to 10 % of their concentration in the plasma.
Plasma was obtained from healthy blood donors from Instituto Português do Sangue (IPS). The concentration used was 10 % (v/v). Distilled and deionised water with a resistivity > 16 MΩcm was used.

4 - FN and ON adsorption studies by AFM

The surface morphology and surface roughness of HA725 and HA1000 discs after FN or ON adsorption was obtained by AFM using a silicon cantilever with a spring constant of 1-5 N/m. For the protein adsorption test 10 µL of FN (20 µg/mL) or ON (10 µg/mL) was added to the referred substrates and incubated during 30 min. Any salts and non-adsorbed protein molecules were washed-off with distilled water. The rinsed surface was dried with a flow of nitrogen, immediately before AFM imaging.

5 - FN and ON adsorption studies by the radiolabelling method

Quantification of FN or ON adsorbed on the HA725 and HA1000 surfaces was performed using the Iodogen method by labeling FN or ON with ^{125}I (^{125}I-FN or ^{125}I-ON). The contribution of free ^{125}I to the total radioactivity found on the nanoHA surfaces was estimated using unlabelled FN solutions at a concentration of 1.0 mg/mL, and an amount of free ^{125}I ion equivalent to that present as ^{125}I ion in the labelled protein solutions. To assess if preferential adsorption of ^{125}I-FN or ^{125}I-ON occurred on nanoHA surfaces, a series of control experiments were performed varying the ratio of labelled to unlabelled FN or ON (10–50%). Protein solutions for adsorption experiments were prepared adding^{125}I-FN or ^{125}I-ON to unlabelled FN or ON to obtain solutions with final activities of ~10^8 cpm/mg. Adsorption tests were performed at 25 ºC placing the

nanoHA substrates in a 24-well tissue culture plate. A drop of 10 µL of ^{125}I-protein solution was added onto each surface, over a period of 60 min. Samples were rinsed three times in PBS and transferred to radioimmunoassay tubes with 500 µL of PBS and surface activity was measured using a gamma counter. Samples were then incubated in PBS over 24 and 48 hrs, to evaluate the rinsing procedure in order to remove both free iodine and non-adsorbed protein. At the end of each immersion time, the samples were rinsed three times with PBS, and then transferred to radioimmunoassay tubes, for gamma activity counting. The surface concentration was calculated by the equation:

$$\text{Protein } (\mu g/m^2) = \frac{counts(cpm) * |\,\text{Protein}\,|_{solution}\,(\mu g/mL)}{A_{solution}(cpm/mL) * SA(m^2)} \qquad (2)$$

where the counts measure the radioactivity of the samples, |protein| solution is the concentration of FN or ON solution, $A_{solution}$ is the specific activity of the respective protein solution, and SA is the actual surface area.

Since there was no statistical difference between 24 and 48 hrs, the immersion time considered was 24 hrs (data not shown). To assess the exchangeability of the adsorbed protein, HA discs were immersed in an unlabeled FN (20 µg/mL), unlabeled ON (0.02 µg/mL) or 10 % plasma solution, over 24 h. The substrates were washed three times with PBS and the residual activity counted. Results reported are the mean ± SD (n=6).

6 - FN exposure of cell-binding domains upon adsorption to nanoHA discs and ON affinity to nanoHA

The exposure of FN cell-binding domains upon its adsorption to nanoHA sintered discs was assessed by immunofluorescence. For that, following incubation in the FN solution (20 µg/mL; 60 min), HA725 and HA1000 discs were rinsed three times with PBS. Samples corresponding to nanoHA discs incubated in PBS without FN were also processed to provide controls for nonspecific antibody binding. After this period of time the samples were fixed in 3.7 % methanol-free formaldehyde, incubated in NH_4Cl (50 Mm; 10 min) and finally in 1 % BSA/PBS for 60 min. Subsequently samples were incubated with the mouse anti-human monoclonal antibody HFN7.1 directed against the major integrin-binding RGD site of human FN (Developmental Studies Hybridoma Bank, Iowa City, IA) diluted at 1:10 000 in blocking buffer (0.25 % bovine serum albumin (BSA), 0.05% Tween-20). After washing in blocking buffer, samples were incubated with a Alexa fluor 488-conjugated rabbit anti-mouse IgG, (Invitrogen,

Molecular Probes), diluted at 1:400, rinsed, mounted with Fluormount and observed in an inverted epi-fluorescence microscope (IFM), (Axiovert 200M, Zeiss, Germany) using Axion Vision Rel. 4.7 software. Fluorescence intensity (FI) was measured for areas with identical size and the microscope settings were kept constant to allow a direct comparison of the values. FI values were determined subtracting the average FI value of nanoHA samples incubated in PBS without protein.

The affinity of ON to nanoHA was evaluated by immunofluorescence using a rabbit anti-human SPARC polyclonal antibody, (Sigma, ref. HPA002989), diluted at 1:100, and a Alexa fluor 488-conjugated goat anti-rabbit IgG, (Invitrogen-Molecular Probes), diluted at 1:500 in blocking buffer (0.25 % BSA, 0.05 % Tween-20). The procedure applied in this immunofluorescence analysis was equal to the one followed for FN.

7 - Cell culture

The effect of pre-adsorption of FN (20 µg/mL) or ON (10 µg/mL) on cell adhesion, viability, and morphology of MC3T3-E1 on nanoHA substrates were analyzed by resazurin test and by IFM after 4, 24, 72 and 96 hrs of cell culture. MC3T3-E1 cells, established as an osteoblastic cell line from normal mouse calvaria, were grown in alpha minimum essential medium (α-MEM, Gibco) supplemented with 10 % (v/v) fetal bovine serum (FBS) (Invitrogen) and 1 % penicillin-streptomycin (Gibco). Cells were cultured in 75 cm^2 plastic culture flasks, and incubated in a humidified incubator (37 ºC and 5 % CO_2). Freshly confluent MC3T3-E1 cells were rinsed with PBS followed by incubation in trypsin/EDTA (0.25 % trypsin, 1 mM EDTA; Sigma) for 10 min at 37 ºC and then resuspended in supplemented medium. HA725 and HA1000 discs were sterilized by immersion in a serial dilute ethanol solutions of 90, 70 and 50% (v/v) during 10 min, and incubated with α-MEM during 30 min. Before cell seeding a pre-incubation step was performed on nanoHA discs and on tissue culture polystyrene (TCPS). The nanoHA substrates were incubated with FN (20 µg/mL), ON (10 µg/mL) or PBS for 60 min. Subsequently cells were seeded on nanoHA substrates and on TCPS commercial 24-well cell culture plates, used as control, at a cell seeding density of $4x10^4$/well. Cells were cultured for periods of 4, 24, 72 and 96 hrs. For each material and culture period, six samples without cells were incubated with complete medium in the same way and used as blanks. The MC3T3-E1 cell distribution and cell morphology on nanoHA substrates was assessed by IFM. Cell-seeded surfaces were rinsed twice with PBS, fixed with 4 % para-formaldehyde for 20 min. After washing with PBS, cells were permeabilized with 0.1 % Triton X-100 for 5 min and incubated in 1 % BSA for 30

min at room temperature. Cell cytoskeletal filamentous actin (F-actin) was visualized by treating the cells with 5 U/mL Alexa Fluor 488 phalloidin (1:40 in BSA 1%, Molecular Probes) for 20 min in the dark. Finally the cells were washed with PBS and cell nuclei were counterstained with 4',6-diamidino-2-phenylindole (Vectashield/DAPI) dye for 10 min in the dark. The images were acquired using an inverted epifluorescence microscope, (Axiovert 200M, Zeiss, Germany) and Axion Vision Rel. 4.7 as software.
MC3T3-E1 cell metabolic activity after cell seeding was evaluated by a resazurin-based assay. [1] For that 50 µL of resazurin (Sigma) at a concentration of 0.1 mg/mL were added onto each well. After 3 hrs of reaction time, 100 µL of supernatant was transferred to the wells of a black-walled 96-well plate. Fluorescence was read using λ_{ex}=530 nm and λ_{em}=590 nm in the microplate reader (Spectra Max Gemini XS, Molecular Devices) using maxPro 4.8 software. The fluorescence value correspondent to the unseeded substrates was subtracted. Results correspond to the mean ± SD of six cultures.

8 - Statistical analysis

Data analysis was performed using R statistical software, version 2.7.1, for windows. Statistical differences were assessed by Student's t tests. Results were considered statistically significant when $p \leq 0.05$.

REFERENCE

1. O'Brien J, Wilson I, Orton T, Pognan F. Investigation of the Alamar Blue (resazurin) fluorescent dye for the assessment of mammalian cell cytotoxicity. Eur J Biochem 2000 Sep;267(17):5421-5426.

Results

1 - NanoHA discs characterization

The diameter and thickness of nanoHA discs (before and after sintering) were acquired and are presented in Fig.1. As expected there was a gradual decrease in diameter as well as in thickness of the HA discs as the sintering temperature increased, namely HA725 and HA1000 shrank 8% (diameter 9.30 ± 0.03 mm) and 23% (diameter 7.77 ± 0.02 mm) relatively to the non-sintered nanoHA disc (diameter 10.14 ± 0.20 mm). The thickness of the samples followed a similar trend.

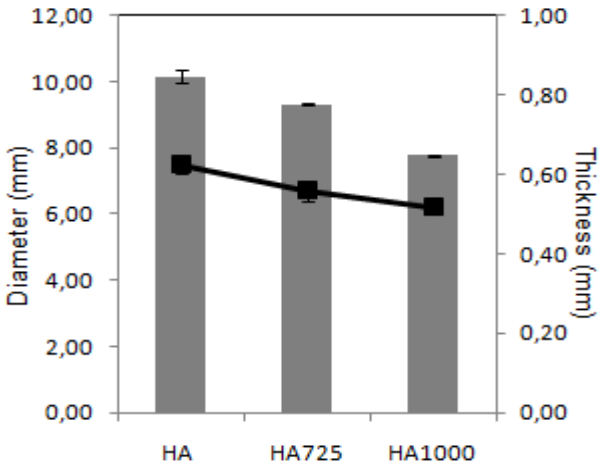

Fig. 1 – Diameter and thickness of HA, HA725 and HA1000 nanoHA discs.

The FT-IR spectra of nanoscale HA, HA725 and HA1000 are represented in Fig. 2. The FT-IR spectrum of nanoscale HA powder was characterized by OH stretching (3570 cm^{-1}) and vibrational (629 cm^{-1}) bands, and PO_4 (υ_3 ~ 1090 and 1037 cm^{-1}; υ_1 ~ 962 cm^{-1}, υ_4 602 and 564 cm^{-1}, υ_2 471 cm^{-1}) bands. One may also observe the characteristics bands of carbonate group, namely the ones corresponding to the υ_3 vibration of C-O (1447 cm^{-1} and 1420 cm^{-1}) and the υ_2 vibrations (875 cm^{-1}). The bands at 3426 cm^{-1} and 1636 cm^{-1} in HA are assigned to lattice water. [1] The FT-IR spectra of the two sintered nanoHA (HA725 and HA1000) showed the same characteristics bands for phosphate, hydroxyl groups and for H_2O observed in the non-sintered nanoHA. The

characteristic bands of the CO_3^{2-} group were observed in nanoHA and HA725. However the HA1000 FT-IR spectrum did not show these bands. In the latter spectrum, the hydroxyl peak detected at 3570 cm^{-1} undergoes a significant increase in intensity (Fig. 2, HA1000) relatively to nanoHA and HA725.

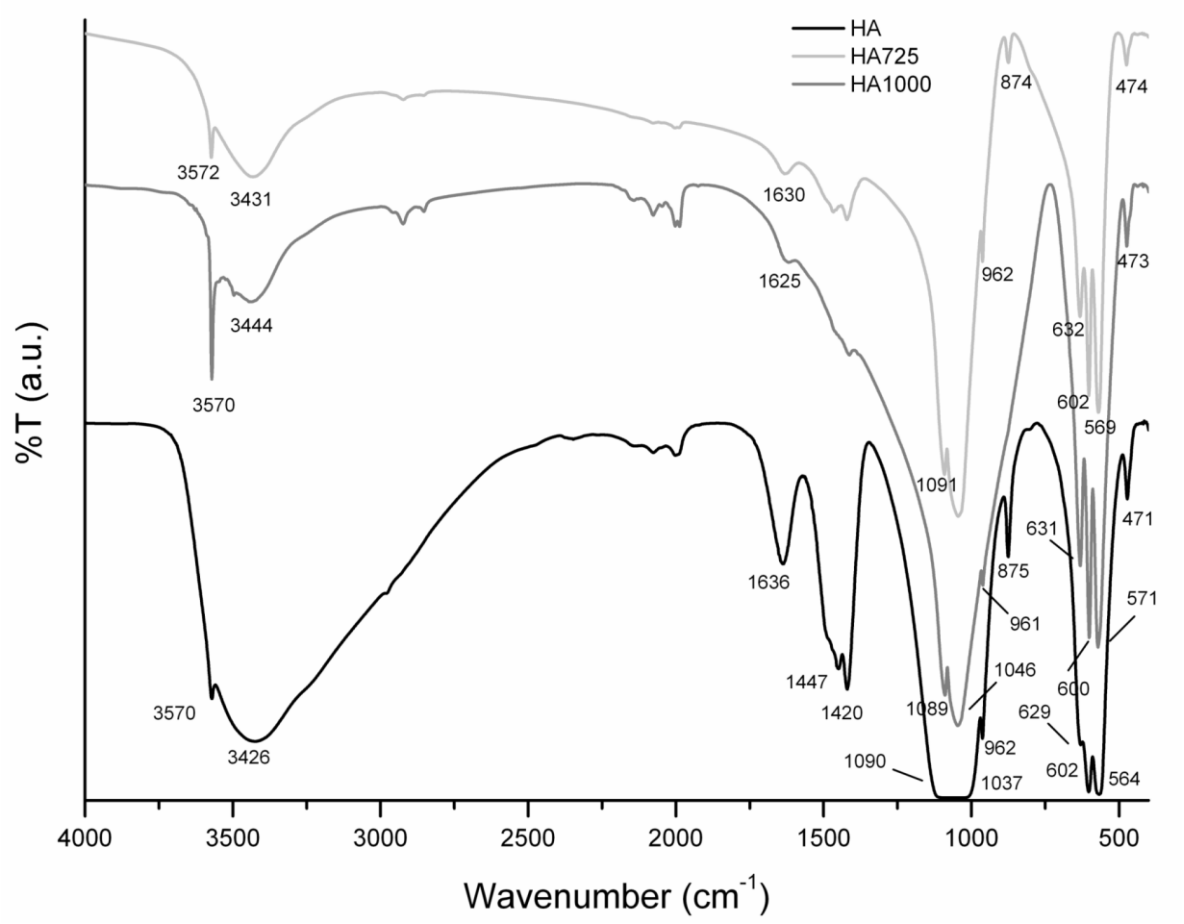

Fig. 2 - FT-IR spectra of nano-scale HA powder (nanoXIM•HAp202), HA725 and HA1000 powders.

The zeta potential (ZP) of HA725 and HA1000 powders in different solutions at physiological pH = 7.4 is shown in Table 1. All ZP values obtained indicate that nanoHA presents a negative net charge in accordance to the negative charge showed by most ceramics. [2-4] Since the two types of sintered nanoHA analyzed revealed ZP values from -7 mV and -33 mV, they have an incipient instability as colloids. For all the electrolytes tested HA725 showed a lower ZP, in terms of absolute value, than HA1000, being more evident for the KCl and H_2O solutions.

Table 1 – Zeta potential values for HA725 and HA1000 powders at pH =7.4 in deionized water, KNO_3 (0.01 M), NaCl (0.01 M), and KCl (0.01 M).

	H_2O		KCl		NaCl		KNO_3	
	ZP (mV)	**RSD (%)**	**ZP (mV)**	**RSD (%)**	**ZP (mV)**	**RSD (%)**	**ZP (mV)**	**RSD (%)**
HA725	-12.5	12.2	-6.65	42.6	-29.5	8.6	-19.3	7.53
HA1000	-23.3	5.48	-25.9	7.61	-32.7	5.81	-21.2	16.5

2 - Surface characterization of NanoHA discs

The results regarding the contact angles of HA1000 and HA725, using ultrapure water as testing liquid, were 17.0 ± 3.0º and 14.3 ± 2.3º respectively. From the low contact angles values obtained, it can be inferred that the substrates have highly hydrophilic surfaces.

Fig. 3 shows SEM micrographs of the HA, HA725 and HA1000 nanoHA surfaces. Before sintering, HA surfaces are mainly constituted by structures of nanoparticles (Fig. 3a). The heat treatment at 725 ºC or 1000 ºC induced the agglomeration of the nanoparticles into grains. HA1000 surface showed a more regular structure, with larger grains when compared to the HA725 surface (Fig. 3 b and c)

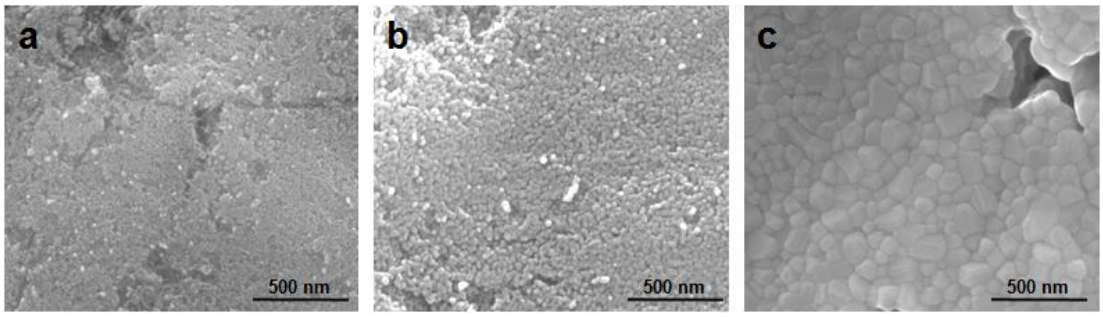

Fig. 3 – SEM images of HA (a), HA725 (b) and HA1000 surfaces (c).

AFM images of the nanoHA surfaces (Fig. 4) revealed morphologic features such as grains that are characteristic of HA structures. The AFM analysis allows the diameter measurement of the HA725 and HA1000 grains, 69.3 ± 20.5 nm and 130.0 ± 49.0 nm, respectively, as mean ± SD.

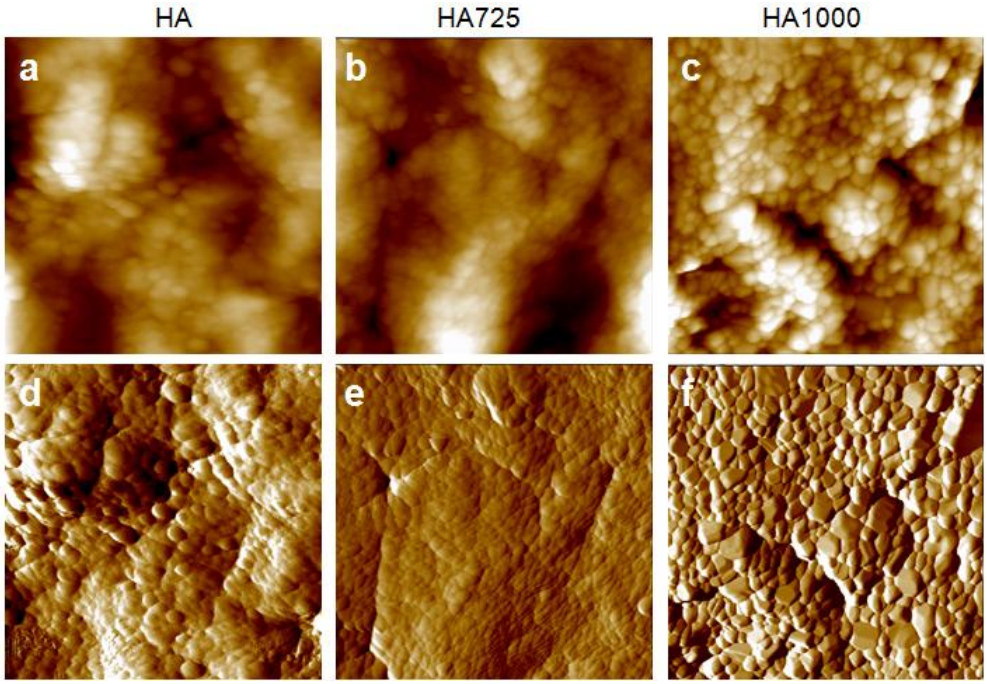

Fig. 4 - AFM topography (a-c) and phase (d-f) images of HA (a, d), HA725 (b, e) and HA1000 (c, f) surfaces obtained in tapping mode (image scale 2500x2500 nm^2).

The surface roughness of HA, HA725 and HA1000 discs was calculated using the SPIP software based on AFM images. Although nanoHA surfaces have presented a distinct topography their root-mean-square roughness (Sq) values were similar as it can be observed in Fig. 5a. The maximum peak with the depth of the maximum valley (Smax) was also measured for the nanoHA surfaces and HA725 surface revealing a higher value (199.3 ± 48.3 nm) when compared to HA (149.1 ± 37.1 nm) and HA1000 (116.7 ± 35.3 nm) surfaces (Fig. 5 b).

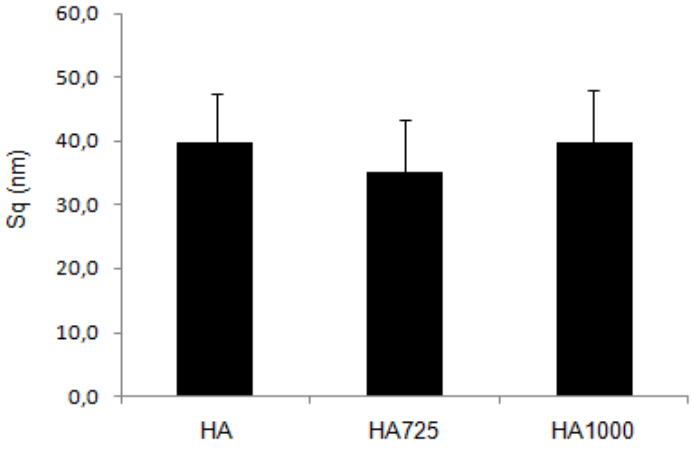

(a)

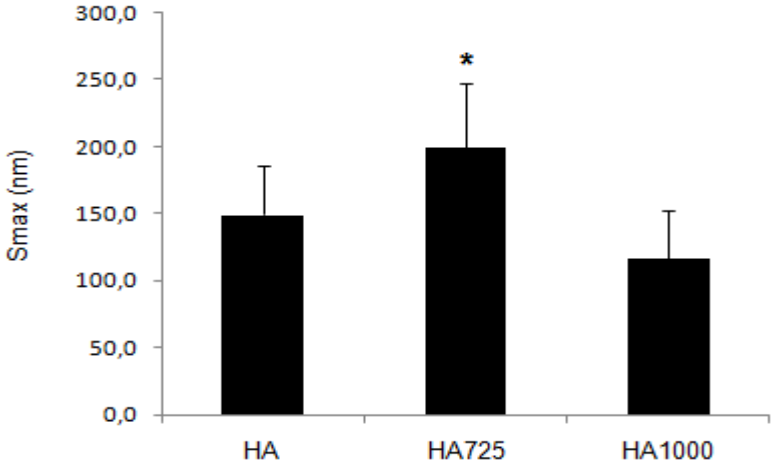

(b)

Fig. 5 –The root-mean-square roughness (Sq) a) and the maximum peak with the depth of the maximum valley (Smax) b) values for HA, HA725 and HA1000 surfaces (scan area: 2500x2500 nm^2). * Indicates a statistical significant difference when compared to HA and HA1000 surfaces ($p \leq 0.05$).

According to the mercury porosimetry data, HA725 showed a significantly higher actual surface area value (46.7 m^2/g), a higher number of pores with a more homogenous pores size distribution and smaller average diameter when compared to HA1000 which actual surface area is 0.5 m^2/g, as indicated by the parameters presented in Table 2.

Table 2 – Data obtained from mercury porosimetry for HA725 and HA1000 discs.

	HA725	HA1000
Pore average diameter (m)	$1.587x10^{-8}$	$6.716x10^{-8}$
Pore volume (cm^3/g)	$8.531x10^{-2}$	$4.106x10^{-3}$
Pore surface area (m^2/g)	$1.841x10^{+1}$	$9.720x10^{-2}$
Pore fraction number	$1.664x10^{-2}$	$8.746x10^{-3}$
Total surface area (m^2/g)	46.705	0.530
Total interparticle porosity (%)	0,380	0,747
Total intraparticle porosity (%)	38.874	2.333

3 - Evaluation of FN and ON adsorption on nanoHA discs as well as surface roughness by AFM

The AFM phase images (Fig. 6 b-c and e-f) obtained after FN and ON adsorption onto HA725 and HA1000, presented a different morphology from the corresponding images of the surface without adsorbed protein (Fig. 6 a and d). Particularly, the ability of phase imaging AFM to distinguish samples with different surface viscoelastic properties enabled the visualization of FN or ON aggregates covering the nanoHA grains, after protein adsorption onto nanoHA substrates. [5]

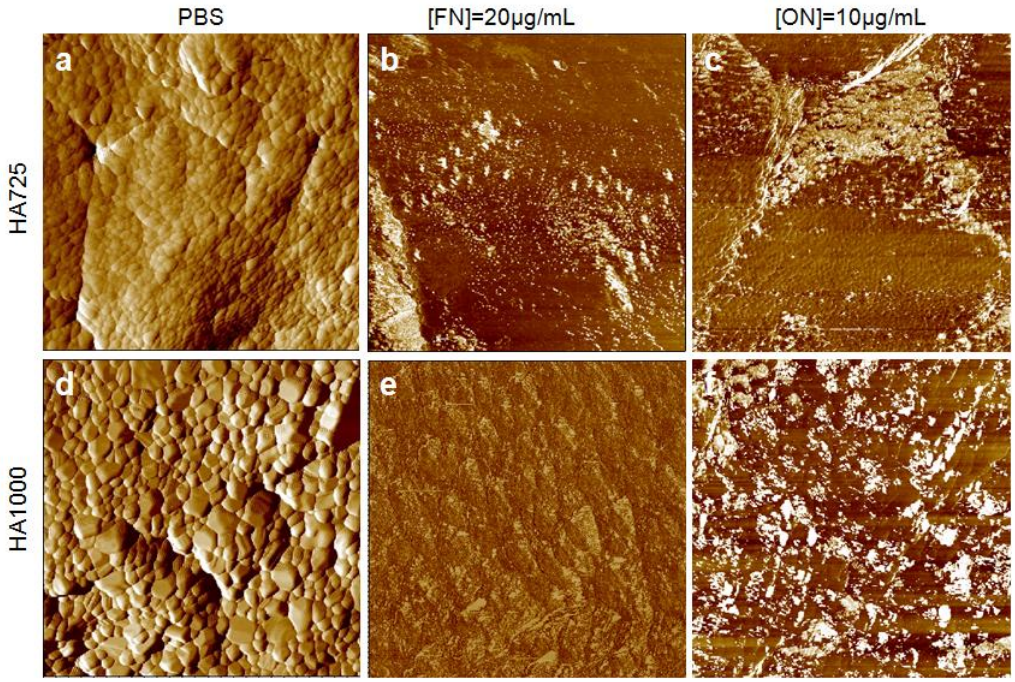

Fig. 6 – AFM phase images of HA725 and HA1000 surfaces before protein adsorption (a, d), after FN adsorption (b, e) and after ON adsorption (c, f) obtained in tapping mode (image scale 2500x2500 nm^2).

The roughness of the HA725 and HA1000 surfaces after protein adsorption was evaluated by the root-mean-square roughness (Sq) and the maximum peak with the depth of the maximum valley (Smax) parameters (Fig. 7).

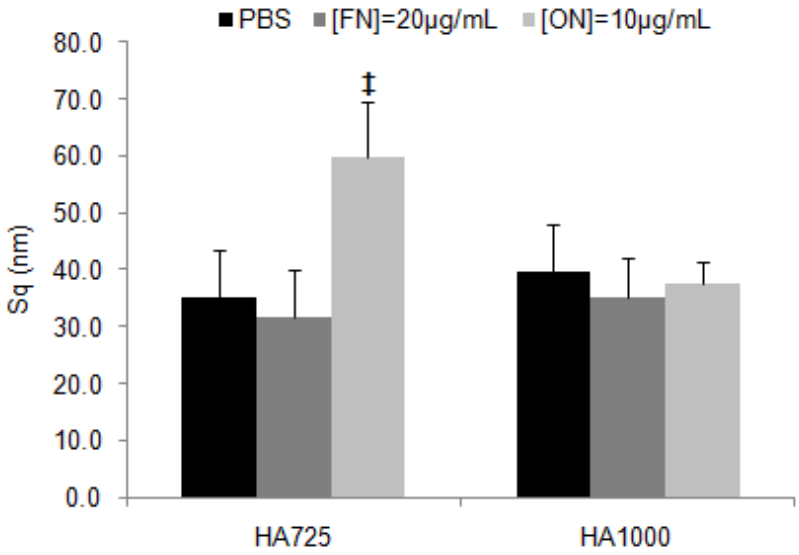

(a)

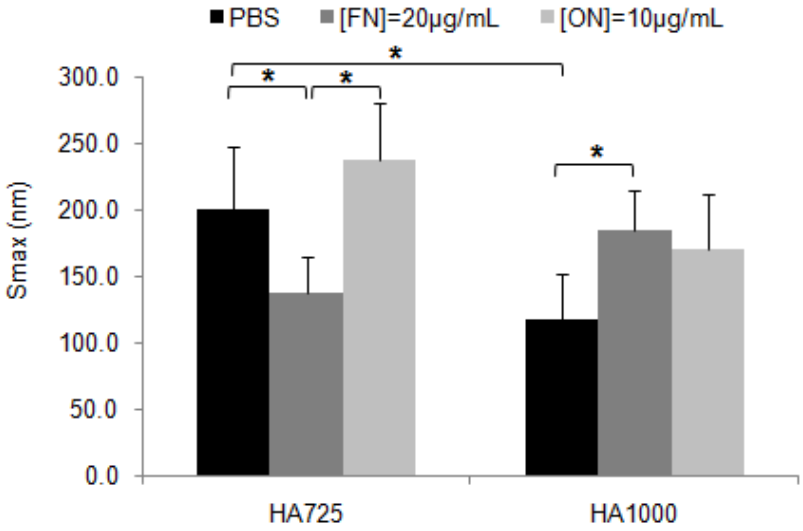

(b)

Fig. 7 –The root-mean-square roughness (Sq) a) and the maximum peak with the depth of the maximum valley (Smax) b) values for HA, HA725 and HA1000 surfaces before protein adsorption, after FN and ON adsorption (scan area: 2500x2500 nm^2). ‡ Indicates a statistical significant difference when compared to any other nanoHA surfaces. * Indicates a statistical significant difference between the two nanoHA discs investigated ($p \leq 0.05$).

In Fig. 7a it can be observed that FN adsorption did not alter the nanoHA surfaces roughness according to the similar Sq values presented by HA725 and HA1000 with and without FN adsorbed.

In terms of Smax values presented in Fig. 7b, after FN adsorption, the Smax of HA725 nanoHA discs decreases, in contrast to the Smax of HA1000 which increases. In the case of ON adsorption, the Sq was higher for HA725 surfaces with ON adsorbed (59.9 ± 9.6 nm) when compared to HA725 without protein (35.1 ± 8.4 nm) or even compared to HA1000 surfaces with and without ON adsorption (37.5 ± 3.8 nm and 39.8 ± 8.2 nm, respectively) indicating that the incoming molecules, as ON aggregates, overgrow on HA725 surfaces. This roughness increase is not so evident in terms of Smax values for HA725 nanoHA surfaces. (Fig. 7b)

4 - Evaluation of FN and ON adsorption on nanoHA discs as well as its exchangeability with FN, ON and 10 % plasma

The adsorption of ON was assessed using ^{125}I-ON. Preferential adsorption of the ^{125}I-labeled ON relative to the unlabeled ON did not occur on the nanoHA surfaces as determined by varying the ratio of the labeled to unlabeled protein in a series of control experiments. A similar trend was observed for the ^{125}I-labeled FN relatively to the unlabeled FN. The adsorption of ^{125}I-ON presented in Fig. 8 shows a significantly higher amount of ON adsorbed to HA1000 surface when compared with HA725 surface.

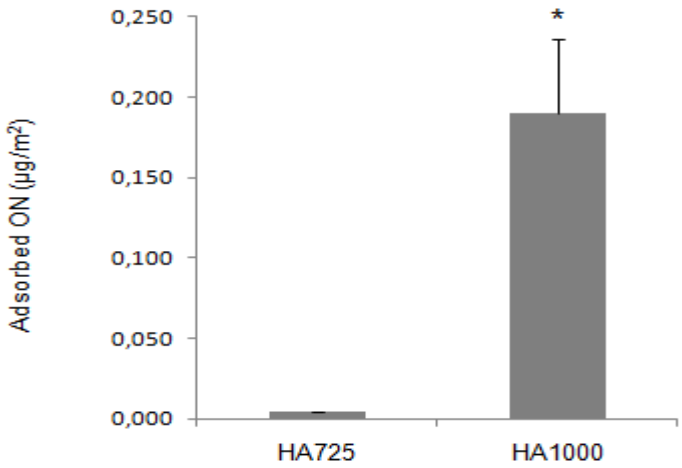

Figure 8 – ON adsorption to HA725 and HA1000 nanoHA discs from a single ON solution (10 µg/mL) labeled with^{125}I-ON. Results presented are the mean ± SD (n = 6). * Indicates a statistical significant difference from HA725 surfaces ($p \leq 0.05$).

It is important mentioning that the concentrations of ON or FN adsorbed onto nanoHA discs were acquired based on actual surface area of substrates, instead of the surface area, calculated from their diameters. Table 3 shows exactly the difference in the values for the amount of ON adsorbed on nanoHA discs surfaces when other the actual surface area or calculated surface area is taken into account.

Table 3 – ON adsorption to HA725 and HA1000 nanoHA discs from a single ON solution (10 µg/mL) radiollabeled (^{125}I-ON). The adsorbed ON concentrations values were obtained based on actual surface area or based on calculated geometric surface area of HA725 and HA1000 discs. Values reported are the mean ± SD (n = 6). *Indicates a statistical significant difference from HA1000 at the corresponding ON concentration measurement ($p \leq 0.05$).

	Adsorbed ON (µg)/actual surface area (m^2)	**Adsorbed ON (µg)/surface area (m^2)**
HA725	0.004 ± 0.001*	179.8 ± 32.0*
HA1000	0.190 ± 0.001	130.3 ± 31.5

The evaluation of FN adsorption on nanoHA surfaces revealed that HA725 surfaces adsorbed lower amounts of FN than HA1000 surfaces, as shown in Fig. 9 (0.013 µg/m^2 and 0.459 µg/m^2 respectively). After the adsorption step from a single FN solutions, desorption was performed with FN washes during 24h, in order to evaluate the exchangeability of FN molecules. Fig. 9 shows that the exchangeability of the pre-adsorbed (^{125}I-FN) for unlabeled FN molecules and unlabeled ON was significantly higher in HA725 surfaces than in HA1000 as shown by the FN concentration decrease (~46 % and ~17 % for HA725 and HA1000 substrates). On the other hand, the amount of FN adsorbed from a single ^{125}I-FN solution on the two substrates was identical to the FN amount adsorbed after soaking in 10 % plasma for 24 h (Fig. 9). These results indicate that HA725 substrate shows a higher reversibility of FN molecules by others FN molecules in the presence of unlabeled FN and unlabeled ON molecules.

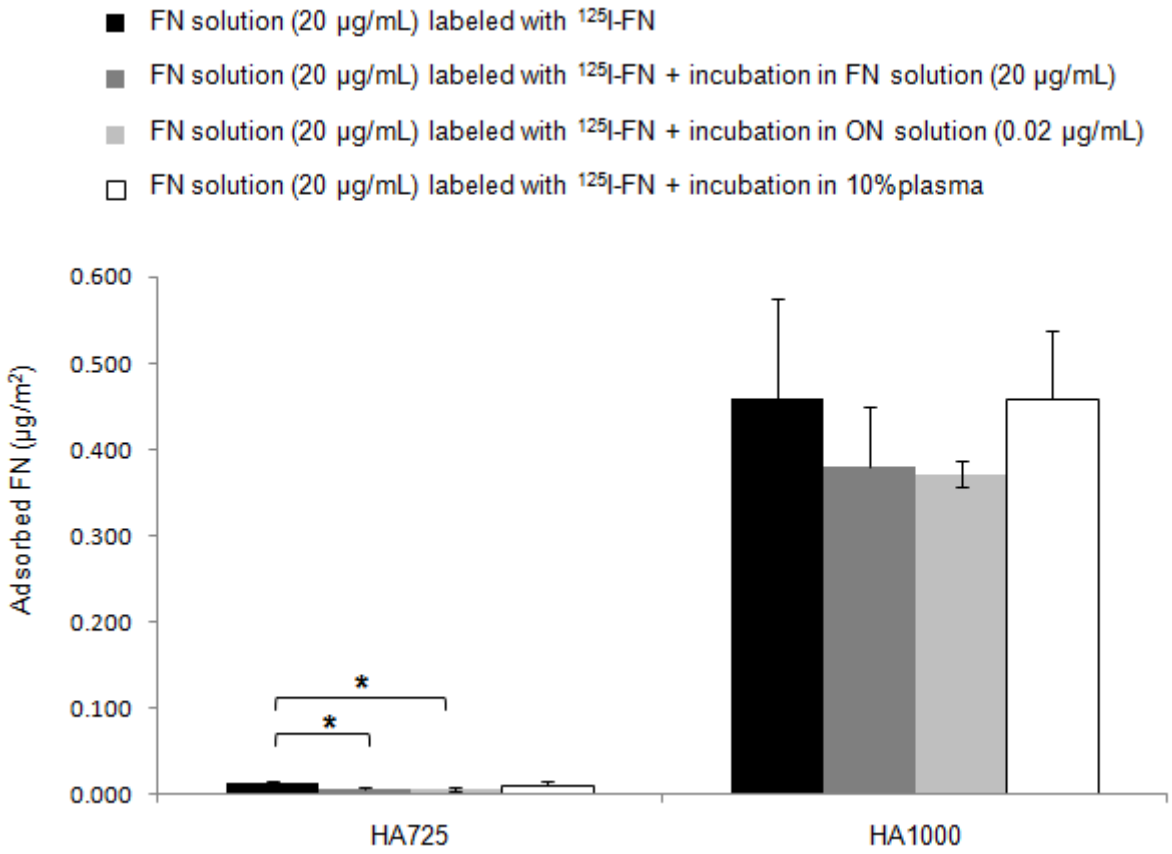

Fig. 9 – FN adsorption to nanoHA surfaces from a single FN solution (20 µg/mL) labeled with ^{125}I-FN and the ability of nanoHA surfaces to exchange FN after incubation in FN (20 µg/mL), ON (0.02 µg/mL) and 10% plasma solutions. Results presented are the mean ± SD (n = 6). Statistical significant higher levels of adsorbed FN were found for HA1000 as compared to HA725 independently of the conditions used. * Indicates a statistical significant difference before and after protein exchangeability ($p \leq 0.05$).

5 – Evaluation of FN conformation on nanoHA surfaces as well as ON affinity to nanoHA surfaces

The results regarding the epitopes distribution of FN by immunofluorescence assay with monoclonal antibody HFN 7.1 for the cell binding domain on FN are present in Table 4.

FN coated discs revealed a homogeneous distribution of FN cell-binding domains for both substrates. The subsequent image analysis revealed for HA1000 substrates significantly higher FI values as compared to HA725, indicating the exposure of a higher number of cell binding domains upon FN adsorption.

Table 4 – Conformation of FN upon adsorption to nanoHA substrates, as probed by immunofluorescence of FN cell-binding domains. Fluorescence intensity/actual surface area values were obtained after IFM imaging and subsequent image analysis. Results are the average ± SD (n=3). * Indicates a statistical significant difference from HA1000 nanoHA surfaces ($p \leq 0.05$).

	FI/m^2
HA725	0.020 ± 0.002 *****
HA1000	0.491 ± 0.001

Table 5 shows the ON affinity values upon adsorption to nanoHA substrates, as probed by immunofluorescence with a SPARC polyclonal antibody. As for the results of protein quantification by ^{125}I-ON, the fluorescence intensity for the HA725 surfaces was lower as compared to HA1000 surfaces.

Table 5 – ON affinity upon adsorption to nanoHA substrates using anti-human SPARC polyclonal antibody in an immunofluorescence assay. Fluorescence intensity/actual surface area values were obtained after IFM imaging and subsequent image analysis. Results are the average ± SD (n=3). * Indicates a statistical significant difference from HA1000 nanoHA surfaces ($p \leq 0.05$).

	FI/m^2
HA725	0.035 ± 0.005 *****
HA1000	0.776 ± 0.212

6 – Influence of pre-adsorption of ON and FN on MC3T3-E1 morphology, distribution and metabolic activity

The MC3T3-E1 morphology, distribution, and metabolic activity after being cultured on nanoHA substrates with and without protein pre-adsorption for the established periods of time were followed by inverted fluorescence microscopy and by the resazurin test. In Fig. 10 it may be seen that after 4 hrs of incubation, MC3T3-E1 osteoblastic cells are

randomly attached to the analyzed surfaces, with distinct cell morphologies depending on the substrate. Therefore, the adherent cells on HA725 surfaces have a spread and expanded cytoskeleton in contrast with the cells elongated with fusiform fibroblastic appearance on HA1000 surfaces. At 24 hrs of incubation it can be observed a similar cell distribution and cell morphology (elongated shape) on both HA725 and HA1000 discs without pre-adsorbed protein.

The cell metabolic activity values for the MC3T3-E1 on HA1000 substrates for the last three time points were similar to the values found on TCPS (control), as shown in Fig. 11. In contrast, to these findings the metabolic activity values for HA725 surfaces did not exceed 2500 RFU (Fig. 11). Despite the equivalent distribution of adherent cells observed for nanoHA sintered at both temperatures at the first two time points, after 24h, higher levels of viability and cell number were found for HA1000 surfaces as compared to HA725 surfaces (Fig. 10 and Fig.11).

After FN (20 µg/mL) pre-adsorption on HA725, a higher number of adherent cells and more spread cells are observed when compared to substrates without FN adsorbed. At 72 hrs of incubation FN adsorption on HA1000 scaffolds improved significantly the metabolic activity of MC3T3-E1 cells (Fig. 11).

For the same incubation period, it is possible to see cells in mitosis state on all surfaces by the visualization of nuclei counterstained with DAPI and cells reached confluency on HA1000 surfaces. At 96 hrs the surfaces were fully covered with cells on both substrates, except the HA725 substrates adsorbed with ON and those without protein adsorption. This pattern of adhesion induced by FN pre-adsorption was not found for the ON (10 µg/mL) on both nanoHA surfaces.

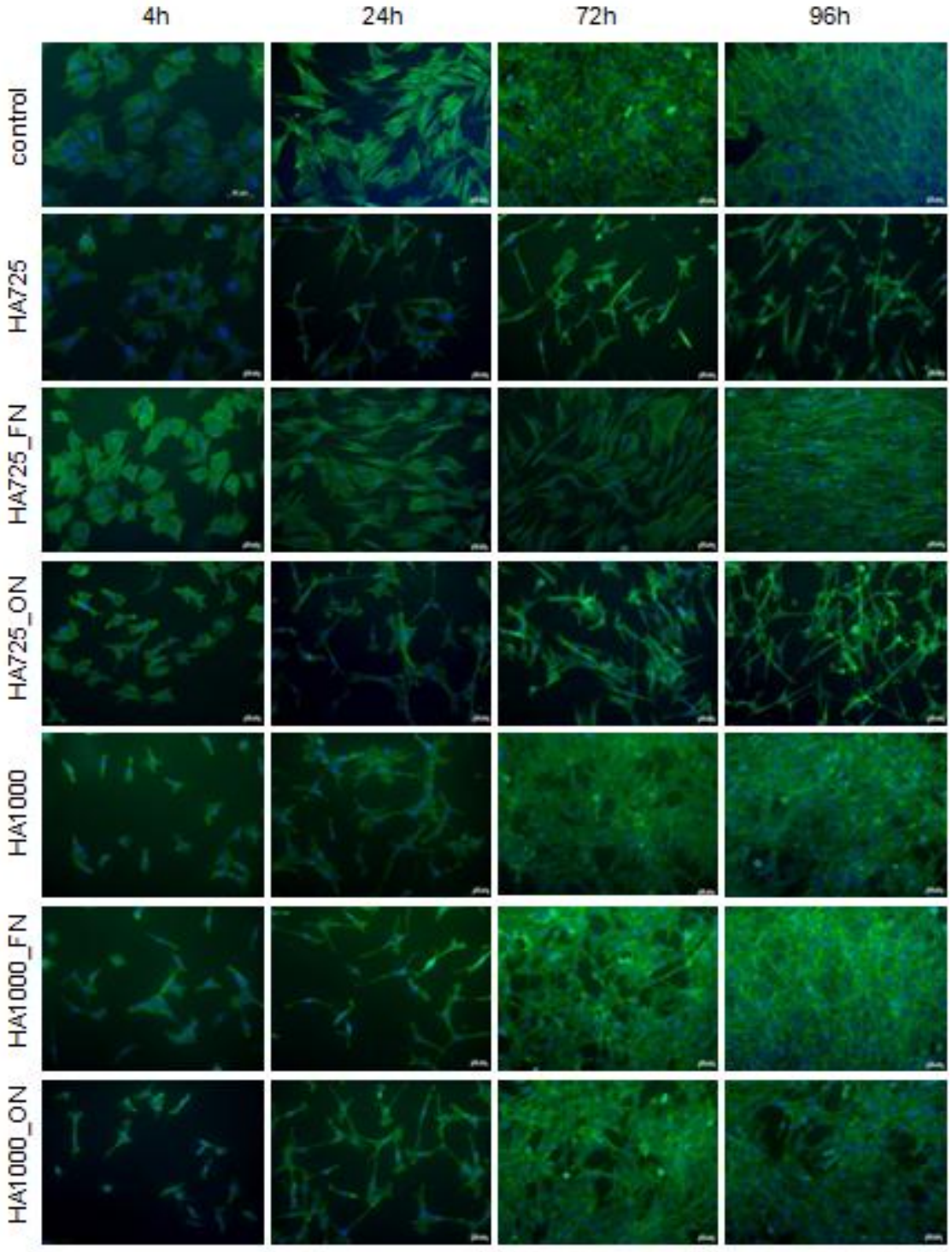

Fig. 10 - MC3T3-E1 cell morphology and cytoskeletal organization on nanoHA imaged with inverted epifluorescence microscope after 4, 24, 72 and 96 hrs without protein adsorption (HA725 and HA1000), with FN (20 µg/mL) pre-adsorption (HA725_FN and HA1000_FN) and with ON (10 µg/mL) pre-adsorption (HA725_ON and HA1000_ON). F-actin is indicated in green while cell nuclei were counterstained in blue with DAPI dye. MC3T3-E1 on TCPS was used as control.

Osteoblast morphology and cell distribution on nanoHA discs upon protein pre-adsorption are in accordance with the results shown by resazurin assay. An identical pattern was observed for the substrates without protein pre-adsorption.

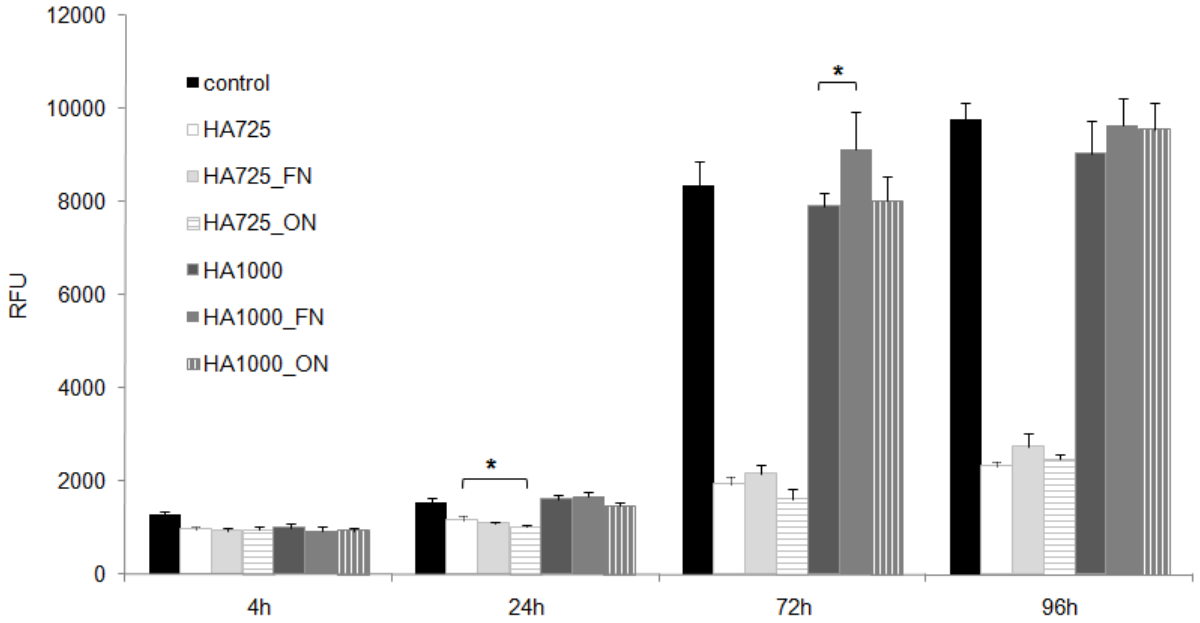

Fig. 11 - Metabolic activity of MC3T3-E1 cultured on nanoHA without and with protein (FN 20 µg/mL or ON 10 µg/mL) pre-adsorption as a function of time. Results expressed in terms of relative fluorescence units (RFU). TCPS was used as control. Values are the average ± SD of six cultures. * Indicates a statistical significant difference before and after protein pre-adsorption ($p \leq 0.05$).

REFERENCES

1. Ribeiro CC, Gibson I, Barbosa MA. The uptake of titanium ions by hydroxyapatite particles - structural changes and possible mechanisms. Biomaterials 2006 Mar;27(9):1749-1761.

2. Lopes MA, Monteiro FJ, Santos JD, Serro AP, Saramago B. Hydrophobicity, surface tension, and zeta potential measurements of glass-reinforced hydroxyapatite composites. J Biomed Mater Res 1999 Jun;45(4):370-375.

3. Suzuki T, Nishizawa K, Yokogawa Y, Nagata F, Kawamoto Y, Kameyama T. Time-dependent variation of the surface structure of bioceramics in tissue culture medium and the effect on adhesiveness of cells. J Ferment Bioeng 1996;81(3):226-232.

4. Suzuki T, Yamamoto T, Toriyama M, Nishizawa K, Yokogawa Y, Mucalo MR, et al. Surface instability of calcium phosphate ceramics in tissue culture medium and the effect on adhesion and growth of anchorage-dependent animal cells. J Biomed Mater Res 1997 Mar;34(4):507-517.

5. Holland NB, Marchant RE. Individual plasma proteins detected on rough biomaterials by phase imaging AFM. J Biomed Mater Res 2000 Sep;51(3):307-315.

Discussion

In our study we used a nanophased HA powder compose by nanoparticles with a typical crystal size of 10 nm to produce dense ceramic scaffolds that conserve the nanoscale dimension and the nanophased HA powder composition. The high actual surface area (SA) of nanophased HA powder, over 120 m^2/g, makes it very difficult to obtain high compactation of the particles during pressing, however it favors the sinterability of HA ceramics. [1] Therefore, it was necessary to establish an adequate combination of parameters related to the compression and sintering procedures to generate the final products. HA725 and HA1000 discs were obtained by applying uniaxial compression stress of 40 bar and two different sintering temperatures, 725 ºC and 1000 ºC with a 15 minutes plateau and applying a heating rate of 20ºC/min. As expected, the heat-treating temperature induced the particles partial melting, resulting in a decrease of the SA and at the same time an increase of the grain size both in HA1000 and HA725 discs (130.0±49.0 nm and 69.3±20.5 nm, respectively). The sintering process did not modify the hydroxyapatite composition of the nanophased HA powder, as confirmed by FT-IR spectra. Despite the different surface area values found for HA725 (46.7 m^2/g) and HA1000 (0.5 m^2/g) ceramics, their surface roughness values were similar, in the range of 30-40 nm. Another morphologic characteristic analyzed for both nanoHA ceramics was porosity. HA725 presented a higher total porosity (39 %), with more homogenous pores and smaller average diameter when compared to HA1000 whose total porosity was 3.1 %. A physico-chemical characterization similar to that of nanophased HA powder was also carried out along the preparation of the bioceramics. Their physico-chemical characteristics are fundamental to interpretate the biological responses and the biointegration of implants. [2] Protein parameters including primary structure, size and structural stability as well as surface properties namely surface energy, roughness, and chemistry have been identified as key factors in the surface-proteins interactions, influencing the protein adsorption and its functional activity. [3-5] Fibronectin (FN) was identified as an extracellular matrix (ECM) protein that not only provides a substrate for cell anchorage but also serves as regulatory protein in processes such as cell adhesion, motility and proliferation. [6] Another glycoprotein that modulates cell proliferation and cellular interaction with ECM is osteonectin (ON), that unlike adhesive proteins such fibronectin, exhibit counter-adhesive effects during tissue repair and differentiation. Osteonectin, also termed

SPARC (secreted protein, acid and rich cystein) as a major non-collageneous bone ECM protein is involved in multiple coordinated functions during bone formation (initiating mineralization and promoting mineral crystal formation). Hence, it is particularly interesting to investigate the adsorption of these two proteins with distinct characteristics on both “as prepared” and sintered nanoHA scaffolds. It is already known that osteonectin has a strong affinity for hydroxyapatite and the region responsible for this binding is the Module I of Osteonectin, the region that is the most distinct from other members of the SPARC gene family. [7] Regarding the results obtained for the ON adsorption on sintered nanoHA discs, the amount of ON adsorbed from a single ON solution of 10 µg/mL was higher on HA1000 (0.190 µg/m^2) than on HA725 surfaces (0.02 µg/m^2). The same tendency was observed for the FN adsorption from a single FN solution of 20 µg/mL, where HA1000 substrates (0.459 µg/m^2) allow for a higher amount of adsorbed FN than HA725 substrate (0.013 µg/m^2). These FN concentration values are lower than the concentrations found by other authors [8-10] and far below the minimum amount of FN required for fibroblast cell adhesion (500 µg/m^2). The reason for this is probably associated with the calculation of protein surface concentration that considers the actual surface area of the analyzed substrates, which is much higher than the geometric surface area. Moreover, the FN molecules adsorbed on HA725 seem to be easily exchanged for unlabeled FN and unlabeled ON than those adsorbed onto HA1000, indicating that FN is less attached to HA725 scaffolds. These findings indicate a relationship between the amount and the binding strength of the FN adsorbed on analyzed nanoHA surfaces that are in agreement with others studies. [11, 12] Many authors have been analyzing the effect of the adsorption of FN to different surfaces in terms of protein structure/conformation, and functional activity involved in cell adhesion, cell spreading and cell migration. [13-15] Namely Dolatshahi Pirous et al [5] in a recent work proposed that the heterogeneous charge present on HA interrupts the native configuration of FN and subsequently a surface-activated unfolding of FN occurs, where the hidden cell binding domain becomes more exposed to the surrounding environment as compared to what happens on the Au reference surface, at a given protein bulk concentration of 20 ug/mL. In the present work immunofluorescent studies with nanoHA surfaces following FN and ON adsorption were performed to evaluate the epitopes distribution of FN as well as the ON affinity to nanoHA surfaces. ON affinity to HA1000 was higher in terms of fluorescence intensity (FI) / actual surface area (m^2) values, as shown by immunofluorescence with SPARC polyclonal antibody (Table 5). The results regarding the epitopes distribution of FN by immunofluorescence assay with monoclonal antibody HFN 7.1 for the cell binding domain on FN revealed for HA1000 substrates significantly

higher FI values as compared to HA725, indicating the exposure of a higher number of cell binding domains upon FN adsorption.

A complete understanding of osteoblast behavior at a biomaterial interface is essential for the clinical application and usefulness of these biomaterials. Indeed, the effect of HA725 and HA1000 surfaces proprieties on MC3T3-E1 cells attachment and metabolic activity after 4, 24, 72 and 96 hrs was examined. At the first two sets of incubation times the osteoblastic cells morphology was dependent to the specific architecture of the substrates. [16] Namely it was observed that on HA1000 surfaces stretched cells with a shrink cytoskeleton were present, in contrast with the cells distributed on HA725 surfaces that had a spread and expanded cytoskeleton. A similar cell distribution on both nanoHA scaffolds was observed for the same periods of time although at 24 hrs the cell metabolic activity for HA1000 surfaces was higher than for HA725. After 24h of incubation the distribution number of cells and the metabolic activity for HA1000 substrates are effectively much higher than for HA725 substrates. Based on the identical metabolic activity values, as well as the surface occupancy, of HA1000 and TCPS it may be conceived that HA1000 is a good candidate material for MC3T3-E1 adhesion, which is a relevant fact in tissue engineering for bone regeneration. The preference of MC3T3-E1 cells for HA1000 surfaces contradicts the results that defend that reduction in grain size induces improvement in osteoblast attachment and proliferation at nanometric range. [17, 18] Nowadays the effort devoted to obtain biomaterials capable of inducing specific cell and tissue response involves not only chemistry modifications of the surfaces but also a biochemical surface modification, immobilizing with proteins, enzymes or peptides. Indeed the role of FN and ON in the attachment and viability of MC3T3-E1 cells on HA surfaces was investigated. ON pre-adsorption on nanoHA substrates did not differ from the results obtained for nanoHA without adsorbed protein, except at 24 hrs for HA725 for which the metabolic activity decreased, indicating that ON did not have anti-proliferative effect on cell culture as observed by others authors. [19, 20] It was interesting to notice the positive influence of FN on cell metabolic activity for HA1000 at 72 hrs and for HA725 at 72h and 96 h, in terms of attached cells number. This osteoblastic adhesion increased when HA was coated with FN, as a rough HA surface was also observed by Despina Deligianni et al. [8] Nevertheless in this work it was observed that MC3T3-E1 cells adhesion was more influenced by nanoHA physical and chemical characteristics than by ON or FN pre-adsorption. In agreement with the fact that the topography could substitute the scaffolds treatment with proteins is Michael Nelson et al [21] that proved that osteoblast adhesion was similar on unfunctionalized nano-crystalline HA compared with

conventional HA functionalized with KRSR (osteoblast selective adhesion peptide). The influence of nanoscale topographic features and protein pre-adsorption on cell behavior is complex and remains to be fully elucidated, varying according to the shape and size of the topographic feature, as well as to the protein and cell type.

REFERENCES

1. Kothapalli C, Wei M, Vasiliev A, Shaw MT. Influence of temperature and concentration on the sintering behavior and mechanical properties of hydroxyapatite. Acta Mater 2004 Nov;52(19):5655-5663.

2. Rouahi M, Champion E, Gallet O, Jada A, Anselme K. Physico-chemical characteristics and protein adsorption potential of hydroxyapatite particles: Influence on in vitro biocompatibility of ceramics after sintering. Colloid Surf B-Biointerfaces 2006 Jan;47(1):10-19.

3. Sousa SR, Manuela Bras M, Moradas-Ferreira P, Barbosa MA. Dynamics of fibronectin adsorption on TiO2 surfaces. Langmuir 2007 Jun;23(13):7046-7054.

4. Shen J-W, Wu T, Wang Q, Pan H-H. Molecular simulation of protein adsorption and desorption on hydroxyapatite surfaces. Biomaterials 2008;29(5):513-532.

5. Dolatshahi-Pirouz A, Jensen T, Foss M, Chevallier J, Besenbacher F. Enhanced Surface Activation of Fibronectin upon Adsorption on Hydroxyapatite. Langmuir 2009 Mar;25(5):2971-2978.

6. Geiger B, Bershadsky A, Pankov R, Yamada KM. Transmembrane extracellular matrix-cytoskeleton crosstalk. Nat Rev Mol Cell Biol 2001 Nov;2(11):793-805.

7. Termine JD, Kleinman HK, Whitson SW, Conn KM, McGarvey ML, Martin GR. Osteonectin, a bone-specific protein linking mineral to collagen. Cell 1981;26(1):99-105.

8. Deligianni D, Korovessis P, Porte-Derrieu MC, Amedee J. Fibronectin preadsorbed on hydroxyapatite together with rough surface structure increases osteoblasts' adhesion "in vitro" - The theoretical usefulness of fibronectin preadsorption on hydroxyapatite to increase permanent stability and longevity in spine implants. J Spinal Disord Tech 2005 Jun;18(3):257-262.

9. Tamada Y, Ikada Y. Effect of preadsorbed proteins on cell adhesion to polymer surfaces. J Colloid Interface Sci 1993 Feb;155(2):334-339.

10. Webster TJ, Ergun C, Doremus RH, Siegel RW, Bizios R. Specific proteins mediate enhanced osteoblast adhesion on nanophase ceramics. J Biomed Mater Res 2000 Sep;51(3):475-483.

11. Amaral IF, Unger RE, Fuchs S, Mendonça AM, Sousa SR, Barbosa MA, et al. Fibronectin-mediated endothelialisation of chitosan porous matrices. Biomaterials;In Press, Corrected Proof.

12. Sousa SR, Moradas-Ferreira P, Barbosa MA. TiO2 type influences fibronectin adsorption. 19th Conference of the European-Society-for-Biomaterials; 2005 Sep 11-15; Sorrento, ITALY: Springer; 2005. p. 1173-1178.

13. Garcia AJ, Vega MD, Boettiger D. Modulation of cell proliferation and differentiation through substrate-dependent changes in fibronectin conformation. Mol Biol Cell 1999 Mar;10(3):785-798.

14. Goldstein AS, DiMilla PA. Effect of adsorbed fibronectin concentration on cell adhesion and deformation under shear on hydrophobic surfaces. J Biomed Mater Res 2002 Mar;59(4):665-675.

15. Michael KE, Vernekar VN, Keselowsky BG, Meredith JC, Latour RA, Garcia AJ. Adsorption-induced conformational changes in fibronectin due to interactions with well-defined surface chemistries. Langmuir 2003 Sep;19(19):8033-8040.

16. Lossdorfer S, Schwartz Z, Lohmann CH, Greenspan DC, Ranly DM, Boyan BD. Osteoblast response to bioactive glasses in vitro correlates with inorganic phosphate content. Biomaterials 2004 Jun;25(13):2547-2555.

17. Smith IO, McCabe LR, Baumann MJ. MC3T3-EI osteoblast attachment and proliferation on porous hydroxyapatite scaffolds fabricated with nanophase powder. Int J Nanomed 2006;1(2):189-194.

18. Webster TJ, Siegel RW, Bizios R. Osteoblast adhesion on nanophase ceramics. Biomaterials 1999 Jul;20(13):1221-1227.

19. Funk SE, Sage EH. Differential-effects of SPARC and cationic SPARC peptides on DNA-synthesis by endothelial-cells and fibroblasts. J Cell Physiol 1993 Jan;154(1):53-63.

20. Hagan S, Hiscott P, Sheridan C, Wong D, Grierson I, McGalliard J. Effects of the matricellular protein SPARC on human retinal pigment epithelial cell behavior. Mol Vis 2003 Mar;9(12-4):87-92.

21. Nelson M, Balasundaram G, Webster TJ. Increased osteloblast adhesion on nanoparticulate crystalline hydroxyapatite functionalized with KRSR. Int J Nanomed 2006;1(3):339-349.

Chapter V

Concluding remarks and Future work

1. Concluding Remarks

The properties of the analyzed nanoHA substrates had an important role in the adsorption behavior of fibronectin and osteonectin. Particularly, the larger grain size, lower actual surface area and porosity present in HA1000 surfaces allowed for a higher amount of protein to be adsorbed. The protein radiolabelling and immunofluorescence studies showed that FN molecules are weakly attached at HA725 surfaces, with a lower number of epitopes exposed. The surface topography of the substrates clearly affected the MC3T3-E1 morphology, distribution and metabolic activity. Despite the equivalent number of bound cells observed for nanoHA treated at both temperatures at the first two sets of time, after 24 hrs, higher levels of viability and cell number were found for HA1000 surfaces as compared with HA725 surfaces. HA1000 substrates present similar behavior of cell viability and distribution of adherent osteoblast as the one found on TCPS cell culture material. ON pre-adsorption on nanoHA substrates with conditions used did not influence the MC3T3-E1 adhesion. On the contrary, FN pre-adsorption improved the number of adherent cells on HA725 surfaces at 72 and 96 hrs and cell metabolic activity on HA1000 surfaces at 72 hrs. Therefore, it may be suggested that the osteoblast cells attachment and metabolic activity seems to be more sensitive to the nature of the surfaces than to the protein adsorbed.

In conclusion, FN and ON adsorption patterns on nanoHA and subsequent response of osteoblast (cell metabolic activity and morphology), depends on the type of nanoHA substrate, being the HA1000 substrate a better candidate for bone tissue engineering than HA725.

1. Future work

The work carried out and discussed in the present dissertation focused on adsorption of two proteins onto nanophase hydroxyapatite substrates. Further analysis of osteonectin behavior regarding nanoHA surfaces is still required since there are few studies on this protein. As an example, other ON concentrations and competition with other proteins would be very useful to assess the influence on osteoblasts adhesion, cytoskeleton organization, proliferation and differentiation.

The conformation of adsorbed proteins is a key factor for the biocompatibility of surfaces. Normally the changes and conformations usually lead to a decrease in functional activity, and consequently to a decrease in cell adhesion. Therefore the use of specific antibodies for regions that modulates the cell anti-proliferation or HA binding can be very useful to evaluate the ON conformation and thus the biological function of this protein when adsorbed on nanophase HA.